from Chuck Kapin 6/28/77 MK.

PETROLOGY AND GEOCHEMISTRY OF THE PALISADES SILL, NEW MEXICO

OPEN FILE REPORT 81

by

Robert P. Cannon

A thesis submitted to the faculty of the University of North Carolina in partial fulfillment of the requirements for the degree of Master of Science in the Department of Geology.

Chapel Hill

1976

Approved by:

PAUL RAGLAND
Adviser

Reader

Reader

OF-81

90 pgs.

ROBERT PAUL CANNON. Petrology and geochemistry of the Palisades sill, New Mexico. (Under the direction of Dr. Paul C. Ragland.)

Sixty five samples were collected along two profiles from the eastward dipping dacitic Palisades sill, the lowest of four to six thick sills cropping out in Cimarron Canyon, Colfax County, Northern New Mexico. Both profiles contain samples from the upper to the lower contact of the sill; one profile is near-horizontal and the other is near-vertical. All samples were analyzed for major elements, Rb, and Sr by x-ray fluorescence and atomic absorption spectrometry. Microscopic petrography was performed on thin sections prepared from twenty representative samples.

The sill exhibits little mineralogical or chemical variation except for Na_2O, Rb, and CaO concentrations. Soda and Rb show a strong negative correlation with CaO. Elemental variation is much greater in samples from the horizontal profile than from the vertical profile, with samples from the horizontal profile showing an indistinct cyclic variation. Approximately 40 percent of the sill is phenocrysts of plagioclase, quartz, and biotite; the remaining 60 percent is a groundmass of orthoclase, plagioclase, quartz, biotite, and magnetite. Quartz phenocrysts are embayed and rounded. Some biotite phenocrysts are altered to chlorite or to sericite, magnetite, and leucoxene. Voids in all types of phenocrysts except quartz and in the groundmass occupy approximately 1 percent of the rock volume.

Chemical and mineralogical data suggest that the magma underwent equilibrium crystallization and that the magma intruded to its present position in subvertical isochemical and isomineralogic "fronts". The phenocrysts apparently crystallized in a deep magma chamber; the ground-

mass, in the higher level sill. Pressure drop on intrusion is a probable cause of quartz phenocryst resorption. Corrosive deuteric fluids are thought to have caused dissolution of previously crystallized minerals to produce the voids.

CONTENTS

page

LIST OF FIGURES

Figure page

LIST OF TABLES

INTRODUCTION

The Palisades sill is the lowest of four to six thick, lobate dacite porphyry sills cropping out in and near Cimarron Canyon, Colfax County, New Mexico. The sill is visible as cliffs just west of Philmont Scout Ranch along U. S. 64 between Eagle Nest and Cimarron, New Mexico (Fig. 1). The sill is approximately 370 m thick and outcrops within an area of 3 km by 3 km. It is roughly concordant with the contacts between underlying Precambrian metamorphic rocks and an overlying Permian to Jurassic sedimentary sequence.

The purpose of this research is to study a large sill of intermediate composition by petrographic and geochemical methods and to model its crystallization history. Sill- or lopolith- like mafic bodies such as the famous Skaergaard intrusion (Wager and Deer, 1939) and Bushveld complex (Hall, 1932) have been studied in great detail. Few large sills of felsic or intermediate composition have been systematically studied, primarily because of their relative scarcity. The Palisades sill, New Mexico is ideal for such a study because the sill dips approximately 12° to the northeast, allowing collection from the lower to upper contacts.

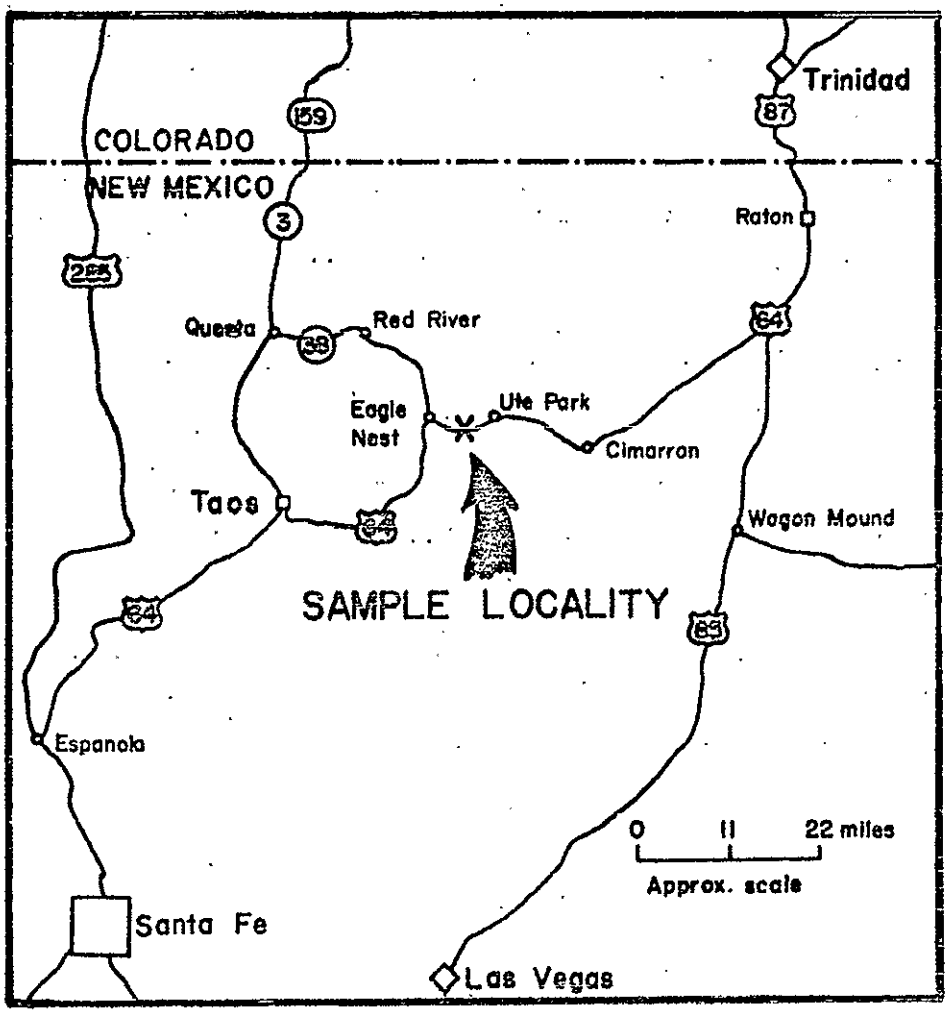

Figure 1. General location of the Palisades sill (after Northrop and Read, 1966, p. 10).

GEOLOGIC SETTING

Previous Work

The most recent mapping of the Palisades sill area was performed by Robinson and others (1964). Previous mapping was done by Smith and Ray (1941, 1943). Smith and Ray (1941, p. 192) classified the sill material as quartz monzonite porphyry and later reclassified it as porphyritic monzonite (Smith and Ray, 1943, p. 904). Robinson and others (1964, p. 50) renamed the dominant rock type in the sills as dacite porphyry. These papers state that the Palisades sill and related sills intruded during the Tertiary, but no other conclusions concerning petrogenesis are given.

Field Relationships

The light colored Palisades sill contains approximately 40 percent phenocrysts of plagioclase, quartz, and biotite in a tan groundmass. The only visible difference in the rock throughout the sill is the amount of quartz phenocrysts, varying in abundance from 1 to 10 percent.

Distinct columnar jointing is found in most parts of the sill.

The sill rests conformably on the top of Precambrian amphibolite (Fig. 2). The contact is distinct and is located within a zone less than 0.3 m wide. No contact metamorphism is visible in the amphibolite and no xenoliths or evidence of assimilation are present in the sill.

The upper contact, observable in the vicinity of Cimarron Canyon,

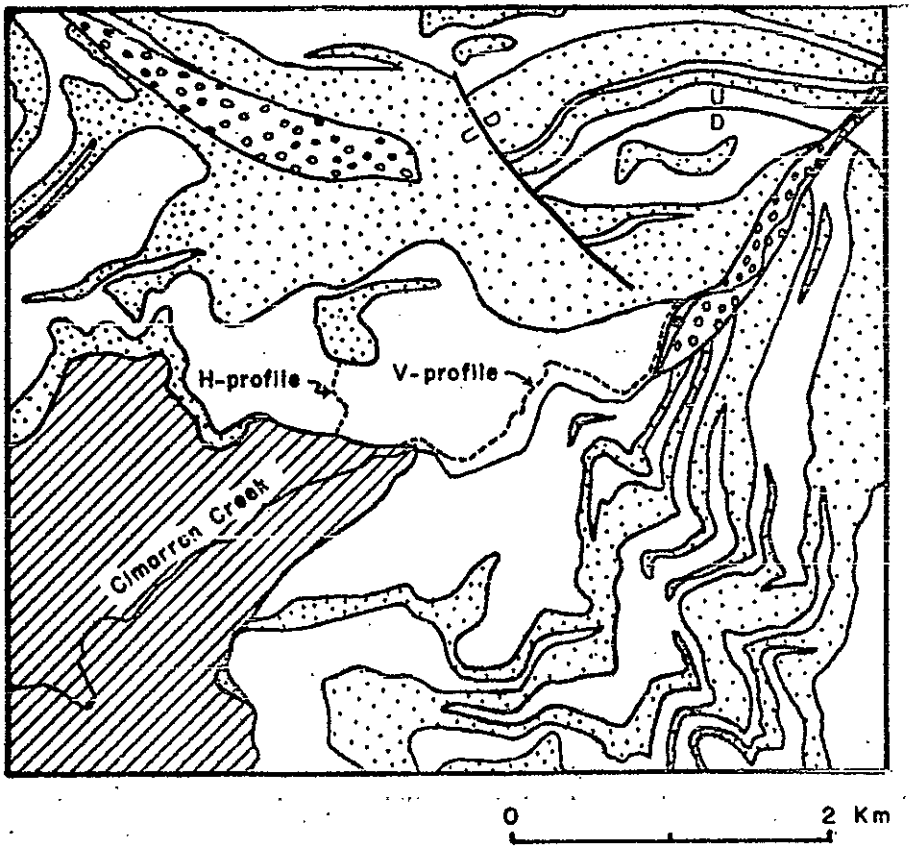

Figure 2. Geologic map of the Palisades sill (containing profiles) and country rocks (after Robinson and others, 1964, Plate 3). White area is Tertiary Palisades sill and related sills. Dotted area is undifferentiated Triassic, Jurassic and Cretaceous sedimentary rocks. Diagonally crosshatched area is Precambrian metamorphic and igneous rocks. Area with circles is Quaternary stream and landslide deposits.

is more vague because it is in an area of less steep topography with a significant soil profile and vegetation. The contact can only be located within 2 to 4 m of "stratigraphic" distance (distance measured perpendicular to contacts). In addition, the upper contact is not strictly concordant with overlying strata, since it cuts contacts between Triassic Dockum Group and Jurassic Entrada Sandstone as well as between Jurassic Entrada Sandstone and Triassic Morrison Formation (Robinson and others, 1964, Plate 3). A 60 to 90 m section of sedimentary rocks separates this sill from the lowermost of the other sills. The sill varies in thickness by about 30 m, having a distinct lobate form and rounding off at its extremities (Robinson and others, 1964, Plate 3). Along the thick central portion of the sill, from which the author collected his samples, contacts strike roughly N10W and dip 12° NE.

GEOCHEMISTRY

Silica, TiO_2, Al_2O_3, Fe_2O_3* (total Fe as Fe_2O_3), MgO, CaO, Na_2O, K_2O, Rb, and Sr were analyzed for all samples. Appendix A tabulates all analyses. Loss on ignition procedure was performed on five samples to check how closely the analyses totaled 100 percent. The mean and standard deviation for the totals of the five analyses are 100.08 $\pm$ 0.65.

Sampling Procedures

Samples were collected along two profiles which extend from the bottom to the top of the sill. One profile, referred to as the H-profile, is roughly horizontal and trends N75E, approximately perpendicular to strike of the sill (Fig. 2). Samples collected along this profile are labeled H1, H2, ..., H40. The other profile, called the V-profile, trends south and plunges 35°. Samples collected along this profile are labeled V1, V2, ..., V25. Samples with larger numbers are progressively nearer the upper contact in each profile.

These two profiles were chosen in hope that any consistent large-scale chemical or petrological variation either vertically or horizontally would be observed. Any large-scale, non-random variation through the sill should be observable except if the isopleths (surfaces of similar mineralogy and chemistry) are parallel to a plane containing the two profiles, that plane striking approximately N75E and dipping 36° SE (Fig. 3).

It would seem plausible that isopleths on intrusion would be

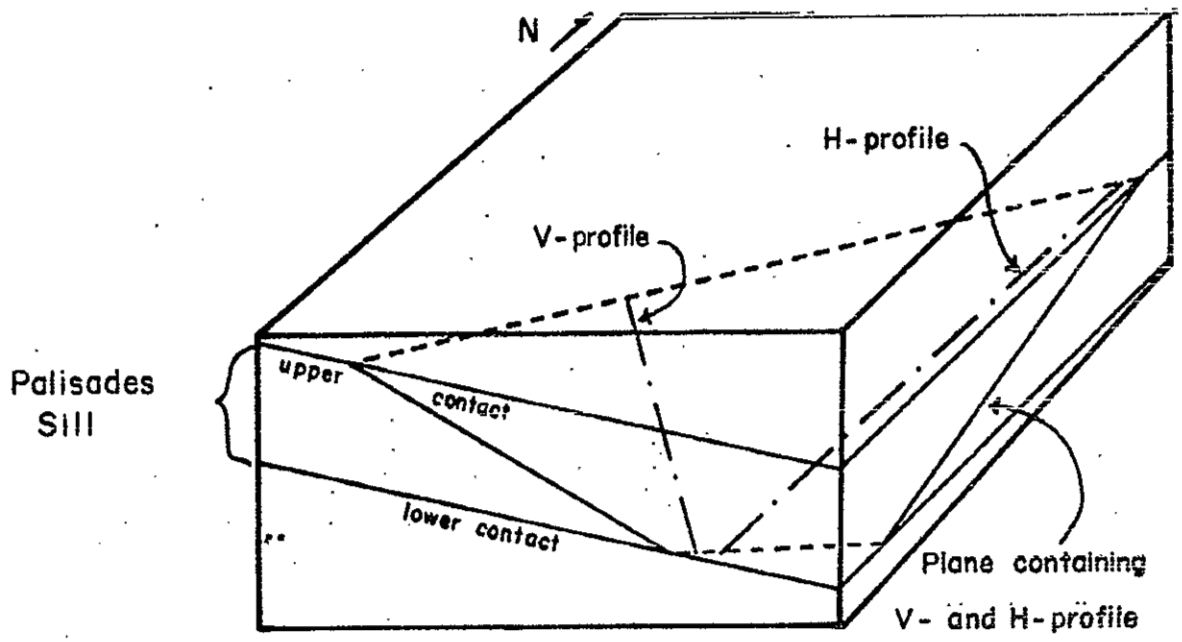

Figure 3. Schematic diagram of the Palisades sill, collection profiles, and planes containing the profiles.

essentially horizontal because of (1) layering of separate sill-like injections, (2) crystal settling and/or floating, or (3) layering due to chill zones of different composition than material near the center of the sill. Conversely, isopleths could be near-vertical and parallel to a feeder dike. If the isopleths are near-horizontal, data from both profiles should show it since both are collected from top to bottom. The H-profile should show any large-scale variation unless the isopleths trend near N75E. V-profile should show variation if the isopleths are not near east-west. From the work of Robinson and others (1964, Plates 3 and 5), the feeders seem to be to the west so that magma intruded eastward. If this is the case, variation from injection "fronts" would be easily recognizable in the H-profile.

Samples from the H- and V- profiles were collected at approximately 15 m and 9 m "stratigraphic" intervals, respectively. Reasons for inaccuracies and irregularities in the locations of sample sites are finding fresh samples in place (i.e., collection site depends on outcrops available) and inherent inaccuracies when locating each site.

The calculated thickness of the sill for the H- and V- profiles is 383 m and 345 m respectively. In order to make correlations along "stratigraphic" levels in the sill, the scale for the V-profile was changed to be 383 m thick, equal to the thickness of H-profile. Appendix B gives the original and, for V-profile, the recalculated distances of sample sites from the bottom of the sill.

Sample Preparation

Samples were checked and trimmed so that no weathered surfaces were used for analysis. The fresh material was subjected to the following:

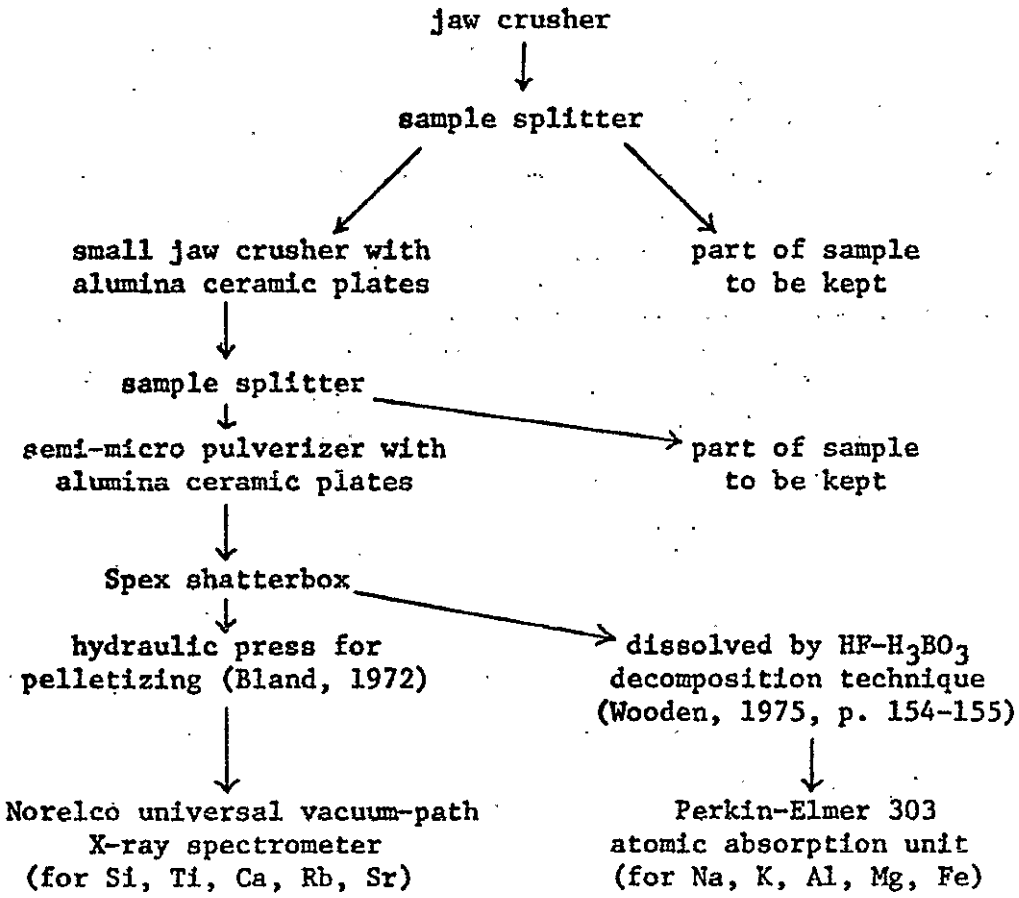

Appendix C gives methods used for the analyses.

Major Elements

From Table 1, Appendix A, and Figures 4 and 5, it is obvious that oxide concentrations vary little over the entire sill, except for samples V23, V24, and V25 whose anomalous values will be discussed in a later section. Table 1 gives the mean, standard deviation, and coefficient of variation for all samples (V23, V24, and V25 excluded from this and subsequent tables unless otherwise noted) and for samples from H- and V- profiles individually. Variation for most elements is greater in the H-profile than in the V-profile; therefore, correlations among elemental concentrations are more apparent in the H-profile.

TABLE 1. MEAN AND STANDARD DEVIATION FOR MAJOR ELEMENTS, Rb, AND Sr.

element or oxide	mean conc.- all samples	σ	V*	mean conc.- H-profile	σ	V	mean conc.- V-profile	σ	V
SiO_2	67.67 %	1.05	1.55	67.62	1.90	2.81	67.75	0.92	1.36
Al_2O_3	15.71	0.31	1.97	15.71	0.32	2.04	15.71	0.30	1.91
Fe_2O_3	2.50	0.16	6.40	2.48	0.12	4.84	2.56	0.21	8.20
MgO	0.68	0.11	16.18	0.66	0.11	16.67	0.71	0.09	12.68
CaO	2.60	0.78	30.00	2.66	0.84	31.58	2.59	0.66	25.48
Na_2O	4.66	0.55	11.80	4.68	0.63	13.48	4.63	0.40	8.64
$CaO+Na_2O$	7.28	0.32	4.40	--	--	--	--	--	--
K_2O	3.29	0.12	3.65	3.31	0.13	3.93	3.25	0.08	2.46
TiO_2	0.28	0.02	7.14	0.28	0.02	7.14	0.29	0.03	10.34
Rb	700 ppm	213	30.43	676	230	34.02	723	175	24.20
Sr	59	4	7.59	59	5	8.47	58	2	3.45

* coefficient of variation = 100 σ/x

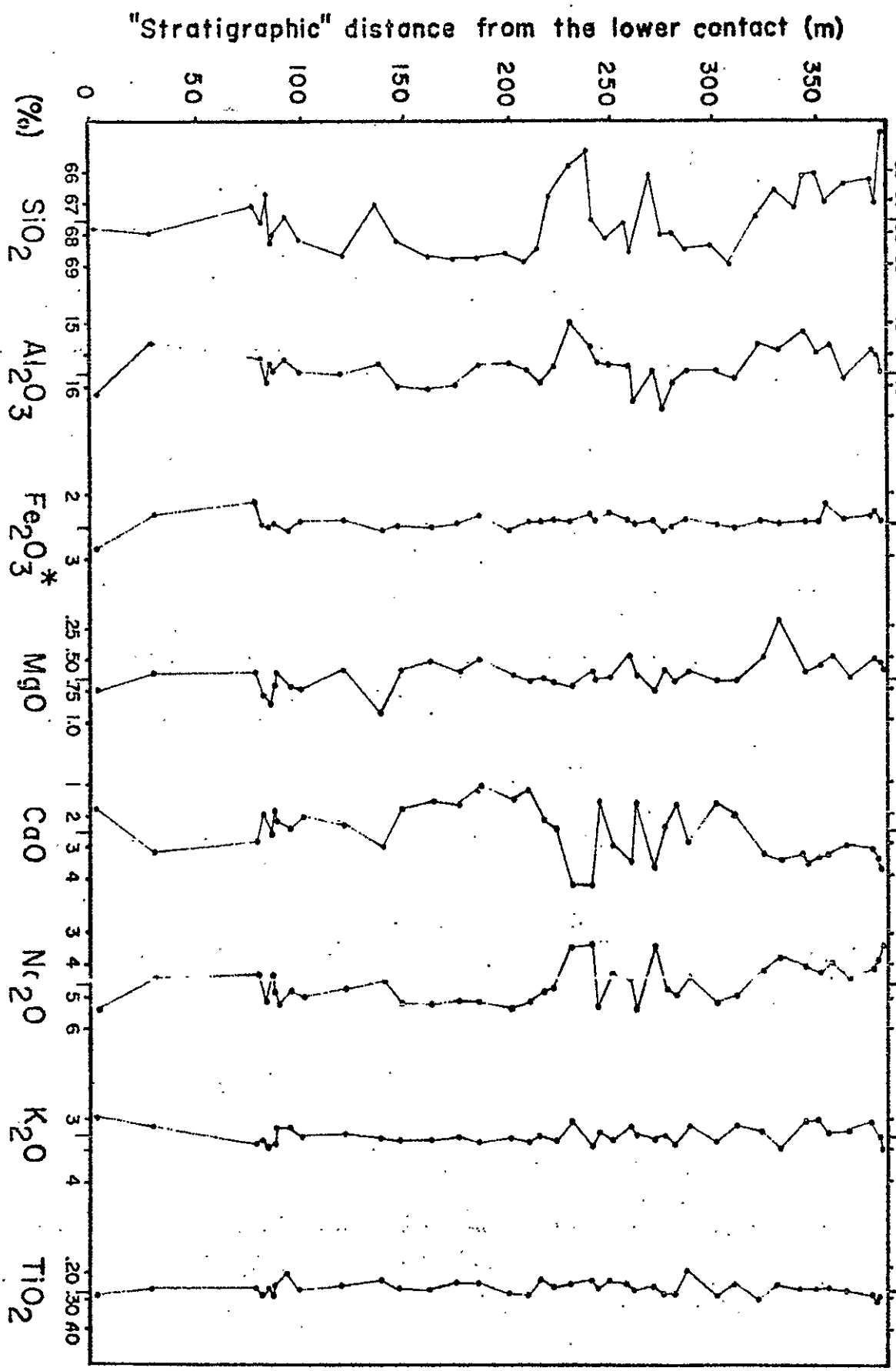
"Stratigraphic" distance from the lower contact (m)
0
50
100
150
200
250
300
350
(%)
SiO2
66 67 68 69
Al2O3
15 16
Fe2O3*
2 3
MgO
.25 .50 .75 1.0
CaO
1 2 3 4
Na2O
3 4 5 6
K2O
3 4
TiO2
.20 .30 .40

Figure 4. Oxide distribution in the H-profile. Longer tic marks on the vertical axes represent the mean values for each oxide.

Figure 5. Oxide distribution in the V-profile. Longer tic marks on the vertical axes represent the mean values for each oxide.

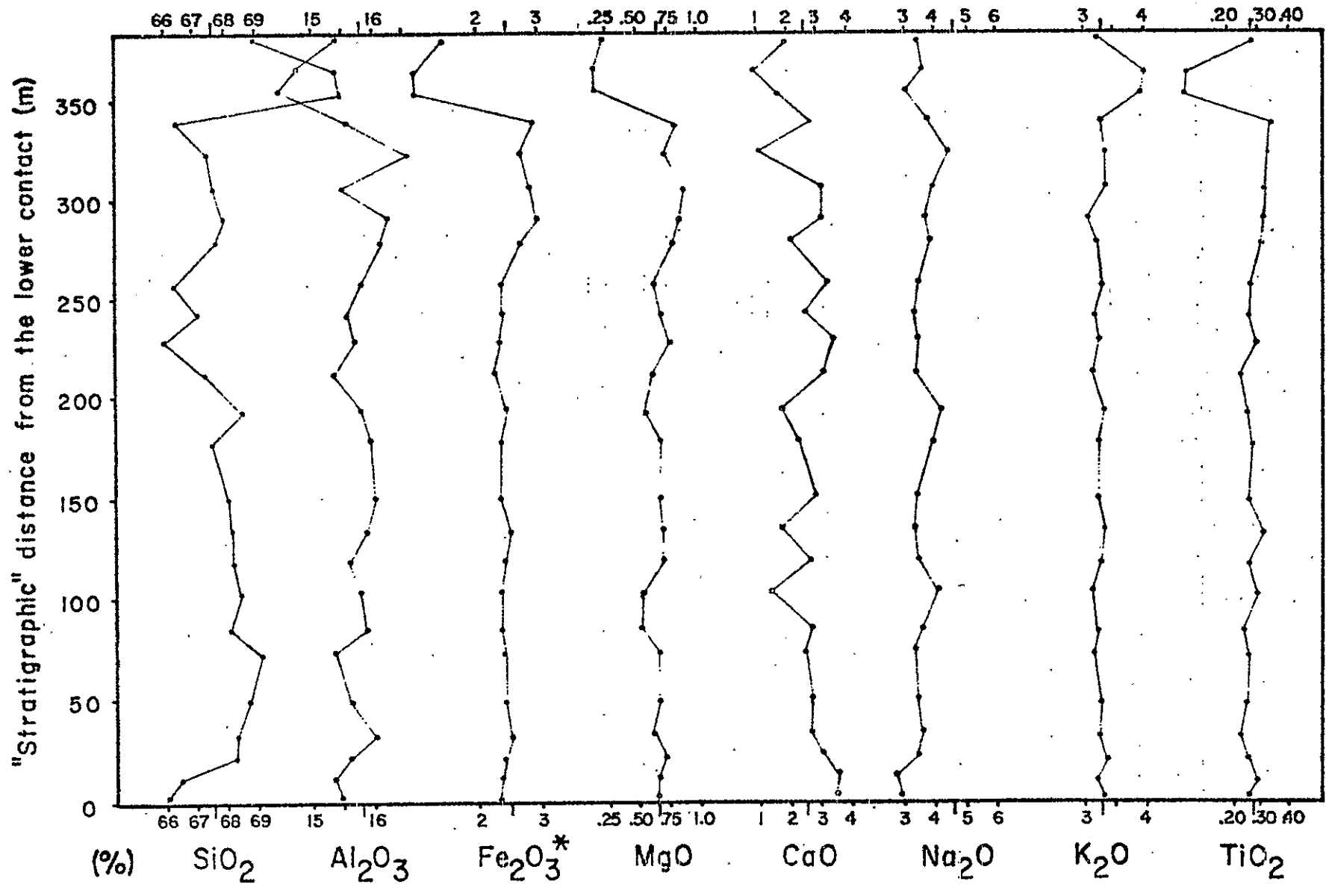
"Stratigraphic" distance from the lower contact (m)
0
50
100
150
200
250
300
350
66 67 68 69
15 16
2 3
.25 .50 .75 1.0
1 2 3 4
3 4 5 6
3 4
.20 .30 .40
(%)
SiO2
Al2O3
Fe2O3*
MgO
CaO
Na2O
K2O
TiO2

The following observations with regard to elemental variations can be made (V23, V24, and V25 excluded) using Figures 4 and 5:

SiO_2 - Variation is quite small. Soda and SiO_2 exhibit a positive correlation; CaO and SiO_2, a negative correlation. Samples V5 and V6 show a minor contradiction to this trend.

TiO_2 - There is insignificant variation except in samples V18 to V22. Percent TiO_2 increases from 0.28 (= TiO_2 mean) for V17 to 0.36 for V22.

Al_2O_3 - Alumina shows a poor positive correlation with SiO_2.

Fe_2O_3* - Total iron exhibits minor variation except for samples V18 to V22. For these samples, Fe_2O_3* is high with values ranging from 2.75 to 3.02 in comparison with a mean of 2.50 and σ of 0.16.

MgO - Magnesia shows more variation than TiO_2 or Fe_2O_3*, but variation is random. Samples V18 to V22 have high values ranging from 0.76 to 0.90 in comparison with a mean of 0.68 and σ of 0.11. Note these high values are from the samples that have high percentages of TiO_2 and Fe_2O_3*. Sample H33 has a low value of 0.24; sample H11, a high value of 0.96.

CaO and Na_2O - These oxides show a strong negative correlation, with $r = -0.95$ (Fig. 6).

K_2O - Potash exhibits little variation. Sample H40 (nearest the upper contact) has a slightly high K_2O value of 3.56 compared with a mean of 3.29 and σ of 0.12.

Normative Analyses

Because chemical compositions are very similar for samples throughout the sill (except V23, V24, and V25), norms calculated from oxide analyses are also very similar. Table 2 gives C. I. P. W. norms of

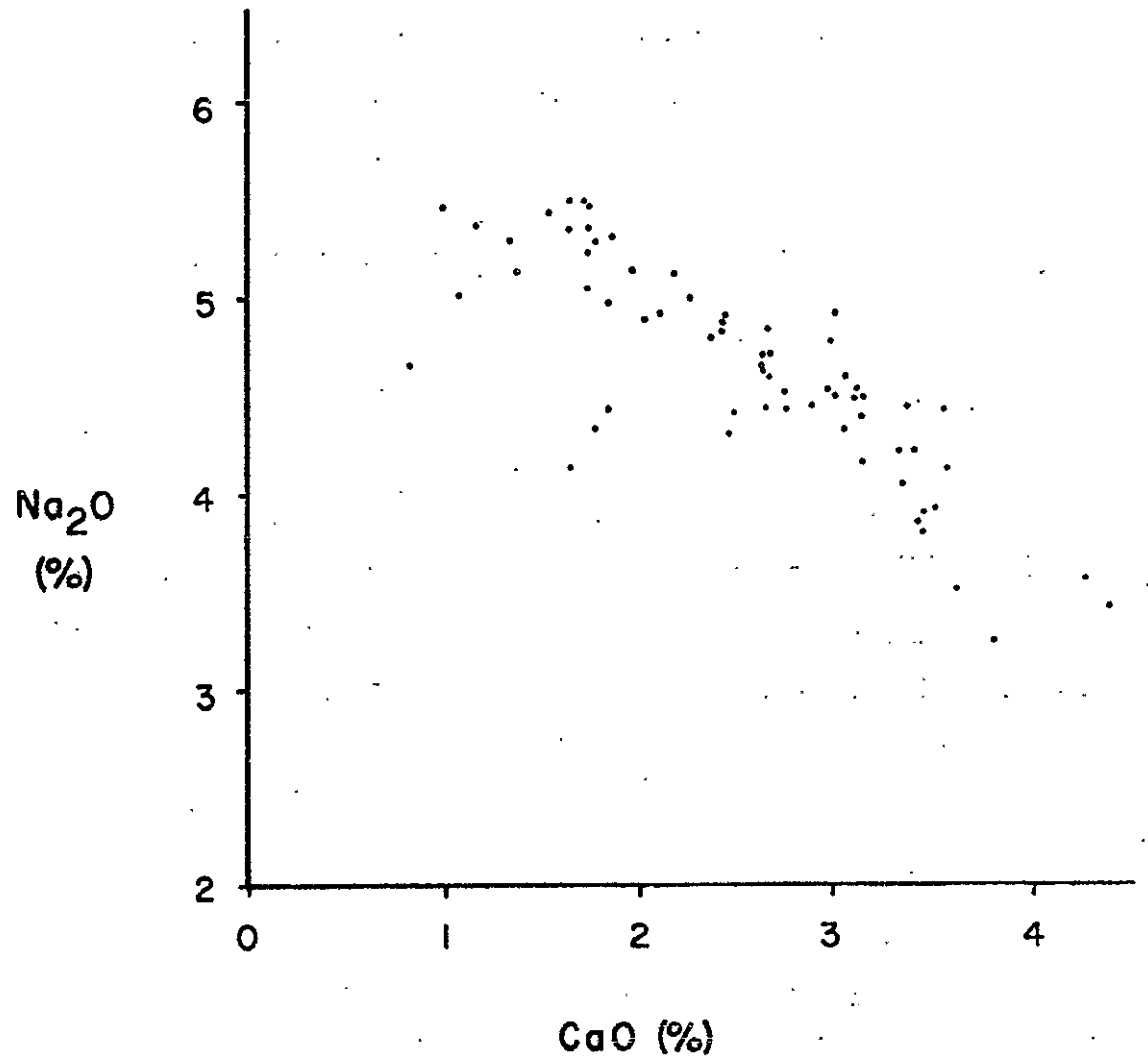

Figure 6. CaO vs Na_2O for all samples.

V23, V24, and V25 and the mean, standard deviation and coefficient of variation for 16 other randomly selected samples. The norms are calculated from data given in Appendix A with total oxides recalculated to total 100 percent.

TABLE 2. C. I. P. W. NORMS.

Normative Minerals (anhydrous)	Mean Values (16 samples)	σ	V	V23	V24	V25
Quartz	21.88	1.63	7.45	29.50	27.94	28.24
Orthoclase	20.28	0.82	4.04	24.16	24.39	19.68
Albite	40.78	4.32	10.59	36.34	40.46	39.10
Anorthite	11.47	2.77	24.15	8.11	3.18	8.40
Diopside*	0.39	0.65	166.67	0.00	0.00	0.00
Hypersthene	1.61	0.35	21.74	0.41	0.41	0.62
Hematite	2.55	0.19	7.45	1.05	1.06	1.56
Titanite	0.71	0.07	9.86	0.18	0.73	0.74
Corundum*	0.33	0.35	106.06	0.26	1.84	1.65

* Average contains both diopside and corundum, although individual norms do not.

Since C. I. P. W. norms calculate only anhydrous minerals, diopside and hypersthene appear in the norm although neither are optically detected in the rock. Fe_2O_3 : FeO ratio was assumed to be infinite. Nevertheless, feldspar and quartz contents will be relatively accurate. In 10 of the 16 calculations, Al_2O_3 is not in excess and the norm includes diopside.

From normative analyses, the sill is composed primarily of dacite; some samples, whose normative quartz is less than 20 percent, are composed of quartz latite-andesite (classification based on Hyndman; 1972, p. 35).

Using data from Appendix A, normative albite and anorthite were calculated and An (Anx100/An+Ab) for the whole rock was determined

for each sample. The An range is extreme, 9.4 for sample V24 to 41.0 for sample H20, with all samples giving a mean of 24.3 and σ of 7.9.

Chemical Comparison with "Typical" Igneous Rocks

The mean oxide percentages for the Palisades sill were compared against contoured frequency diagrams (oxide percentage versus differentiation index) prepared by Thornton and Tuttle (1960) using the 5000 analyses in Washington's (1917) tables. Differentiation index is the sum of three normative minerals, quartz, orthoclase, and albite, and is 80 to 85 for most Palisades sill samples.

For SiO_2 versus D. I. (differentiation index), Palisades sill samples plot at the contour maximum in the SiO_2 oversaturated region but in a higher SiO_2 and D. I. range than typical dacite, approximately in the rhyodacite-rhyolite area (Fig. 7). This discrepancy is a result of the Palisades sill's having a lower percentage of femic minerals than typical dacite. In addition, its high Na_2O content causes the rock name, dacite, to be somewhat misleading from the rock's real composition.

Potash, MgO, Fe_2O_3*, and Al_2O_3 plot near the center of the contour maximum on their respective oxide versus D. I. diagrams (Table 3). Na_2O and CaO are slightly high for D. I. = 80 to 85, but both are within the maximum.

Rubidium and Strontium

Rubidium varies greatly over the sill, with a range of 251 to 1080 ppm (Fig. 8). The mean for all samples is 694 ppm and σ is 210. Variation is non-random and the only correlation that can be made with other oxides is a poor positive correlation between Rb and Na_2O ($r = +0.65$). No correlation can be drawn between Rb and K_2O ($r = -0.10$),

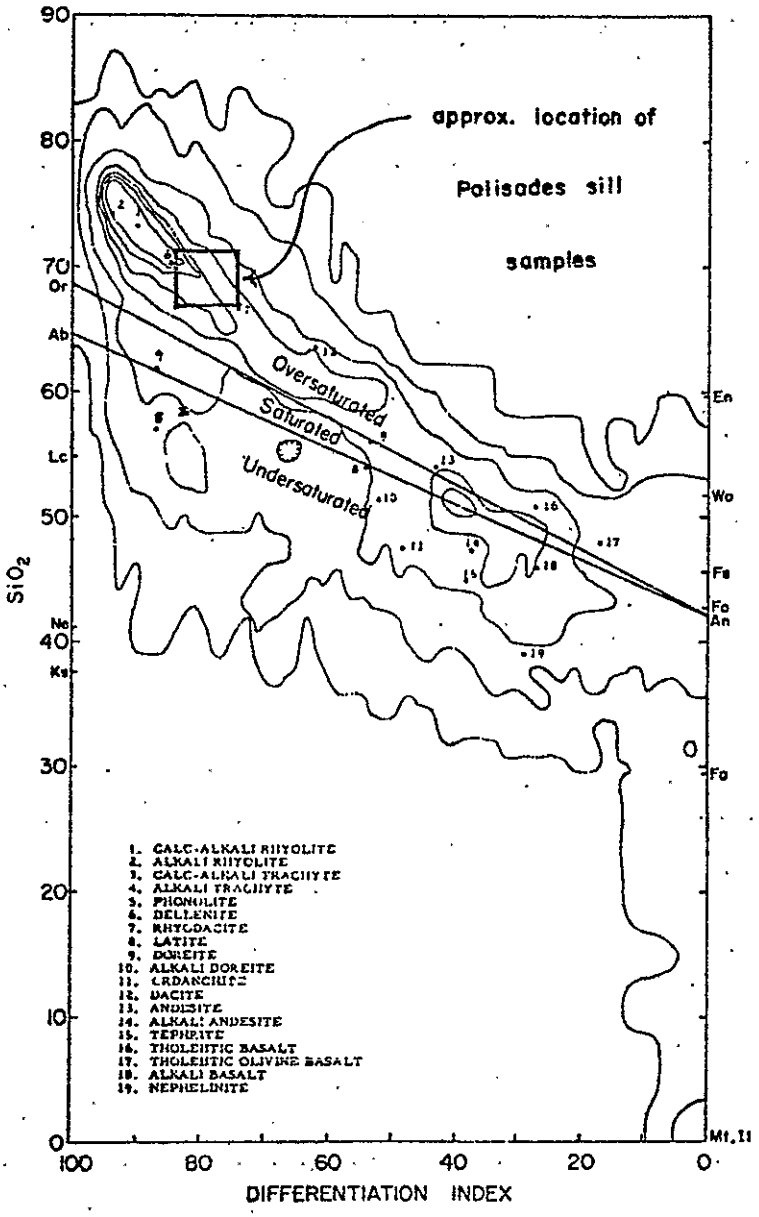

Figure 7. Silica / differentiation index plot for Palisades sill and "typical" igneous rocks (after Thornton and Tuttle, 1960, p. 675).

Figure 8. Rb and Sr distribution in the H- and V-profile. Longer tic marks on the vertical axes represent the mean values for each oxide.

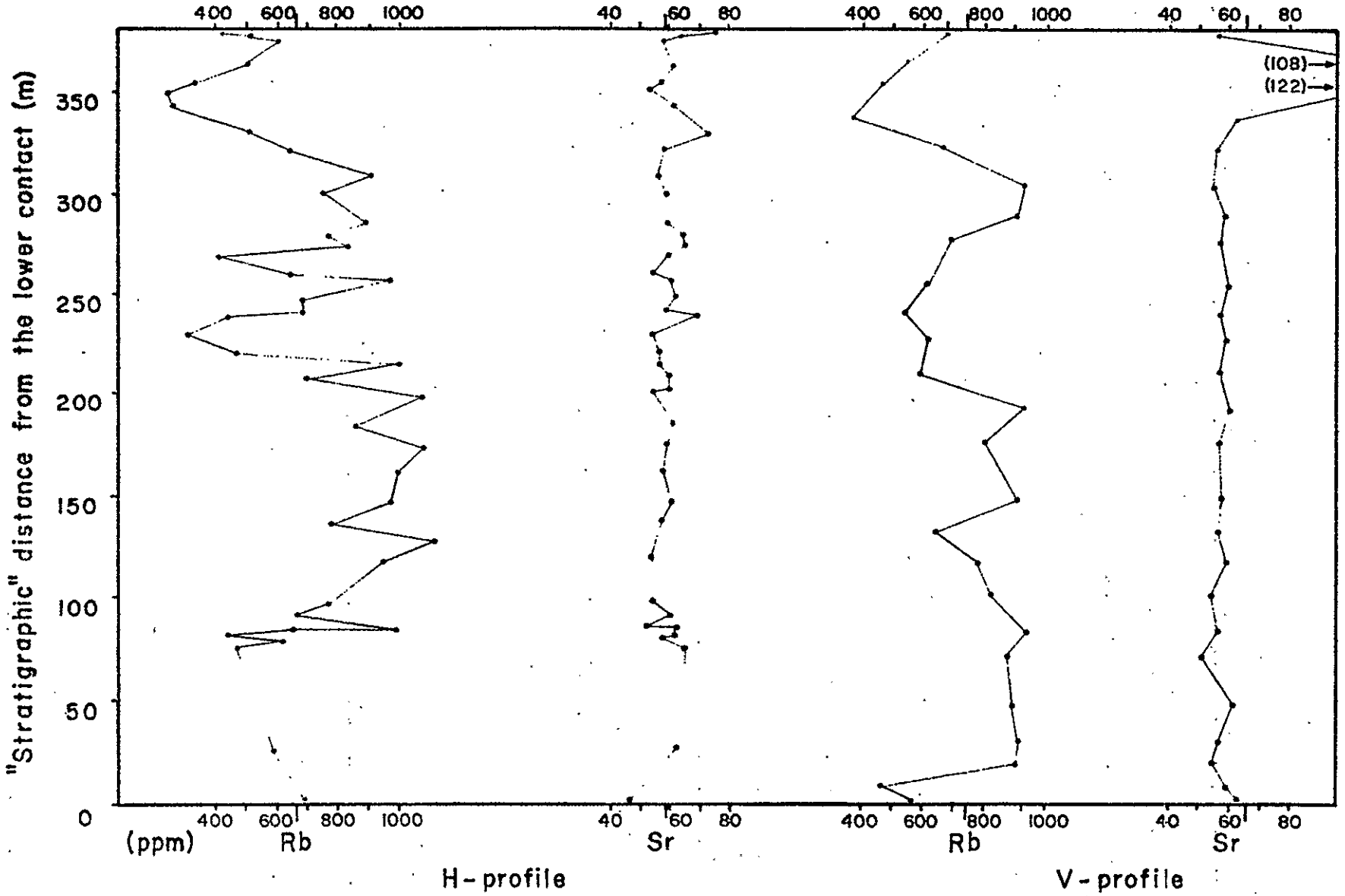
"Stratigraphic" distance from the lower contact (m)
0
50
100
150
200
250
300
350
400
600
800
1000
40
60
80
(ppm)
Rb
Sr
H-profile
V-profile
(108)
(122)

which is contrary to general observations of igneous rocks since K and Rb are chemically very similar (Taylor, 1965, and Tauson, 1965, p. 229). Potassium is extremely invariant, and it is obvious that Rb and K_2O concentrations cannot be directly related.

TABLE 3. OXIDE DISTRIBUTION - "NORMAL" IGNEOUS ROCKS VERSUS PALISADES SILL SAMPLES

	Approximate maximum range from Thornton and Tuttle (1960) (%)*	Mean for Palisades sill samples (%)
SiO_2	66.7 - 70.0	67.7
Al_2O_3	12.5 - 16.9	15.7
Fe_2O_3*	1.0 - 5.0	2.5
MgO	0.0 - 1.3	0.7
CaO	1.0 - 3.2	2.6
NaO	3.5 - 4.7	4.7
K_2O	2.5 - 6.3	3.3

*differentiation index = 82.5

The amount of Rb is quite unusual, especially with the moderate amount of K_2O present. The K/Rb ratios for the Palisades sill (12 to 52, generally less than 30) are extremely low, a Rb enrichment which must have been produced from an anomalous source rock. Taylor (1965, p. 144) notes that "normal" K/Rb ratios are typically 150 to 300.

Rb variation is much greater in the H-profile than in the V-profile (Fig. 8). The mean and standard deviation for each are given as follows:

	Rb (ppm)	σ
H-profile	676	230
V-profile	744	174

Strontium varies little over the sill, from 52 to 75 ppm with a mean of 58.6 ppm and σ of 4.4 (excluding samples V23 and V24, which

are 122 and 108 ppm respectively). A slight positive correlation exists between Sr and CaO ($r = +0.37$), as expected for "granitic" rocks (Turekian and Kulp, 1956, p. 245).

Sr variation for the H-profile is greater than for the V-profile. The mean and standard deviation for each profile are given as follows:

	Sr mean (ppm)	σ
H-profile	59.2	5.1
V-profile	57.6	2.5

PETROGRAPHY

All samples contain phenocrysts of plagioclase (An less than 50), quartz, ±biotite, ±chlorite, and ±magnetite in a submicroscopic to microscopic groundmass of crystalline material. The groundmass for only two samples (V19 and V22) is coarse enough so that individual crystals are distinguishable with a petrographic microscope.

All types of phenocrysts include smaller crystals of all other types of phenocrysts except for the absence of quartz in biotite, which may be obscured by biotite alteration. The most common inclusion recognized is biotite in plagioclase (Fig. 9), suggesting that plagioclase has nucleated around small biotite crystals. These relationships suggest that all the phenocrysts began to crystallize at about the same time and at approximately the same temperature. It is assumed that magnetite crystallized at all stages of magma crystallization because 1) several primary magnetite inclusions are observed in quartz, plagioclase, and biotite phenocrysts, and 2) magnetite crystals are of variable sizes in the groundmass.

Modal analyses were performed on twenty thin sections. As shown in Table 4, the variation in percentages of groundmass and phenocrysts (except quartz) for all samples is small enough that the standard deviation is less than percent reliability as determined from Van Der Plas and Tobi (1965). Modal quartz percentages vary more than other phenocrysts (from 1 to 10 percent) and no correlation can be made with "stratigraphic" position. Variation in percent SiO_2 in the

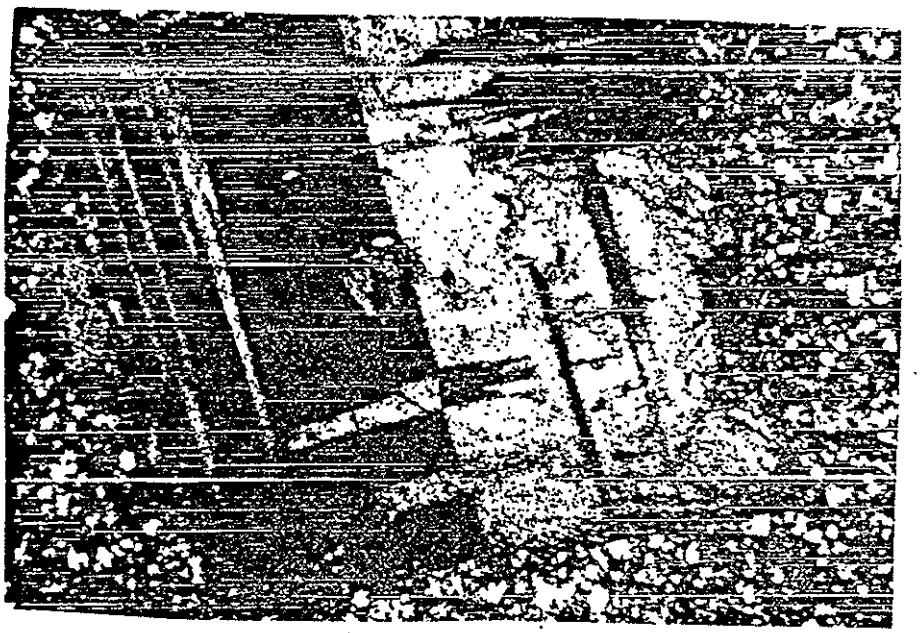

Figure 9. Biotite inclusion in plagioclase. Crossed nicols; field of view, 2.1 mm wide.

whole rock cannot be correlated with percent quartz phenocrysts. Phenocryst percentages have no apparent relationship to whole rock chemical variations.

TABLE 4. MODAL DATA FROM TWENTY THIN SECTIONS

		Mean	σ	Percent Reliability
Phenocrysts	Groundmass	60.1	3.2	4.5
	Quartz	6.0	2.4	2.0
	Plagioclase	28.9	2.7	4.0
	Biotite	4.0	1.1	1.5

Of the twenty thin sections examined (every fourth sample in the H-profile and every third sample in the V-profile), two contain xenoliths. A small amphibolitic xenolith approximately 19 mm wide in sample V19 contains hornblende with some magnetit. and plagioclase. It does not appear to have reacted with the magma. Sample V16 has a 16 mm wide xenolith or autolith of a single quartz crystal containing a euhedral but highly altered feldspar inclusion and a euhedral biotite inclusion. The quartz crystal contains and is surrounded by sericite.

Plagioclase Phenocrysts

Plagioclase phenocrysts are equant and range in width from 0.5 to 3.0 mm. Most of the larger crystals are euhedral to subhedral, many containing albite, pericline and Carlsbad twinning. Several thin sections have zoned phenocrysts. Some plagioclase apparently nucleated from small biotite crystals as demonstrated by numerous biotite inclusions (Fig. 9).

Plagioclase crystals vary from having narrow "cloudy" rims and distinct twinning to being completely disrupted in which no twinning

is visible and interference figures are indistinct or not obtainable. Within a single thin section, all plagioclase crystals are altered to the same degree. No correlation can be made between degree of alteration and sample location.

Determination of the An-content of plagioclase phenocrysts was attempted by two methods, by Michel-Levy's method and by chemical analyses of drilled out plagioclase phenocrysts. Michel-Levy's method is of no value for Palisades sill samples. Too few albite-twinned crystals were of suitable orientation (less than five) to make the method statistically valid. Phenocrysts of samples H17 and H25 have An values of 35 and 44, respectively, as determined by atomic absorption analyses.

The amount of K_2O in plagioclase phenocrysts is high, indicative of a relatively high temperature of crystallization (Tuttle and Bowen, 1958, p. 131). On a ternary diagram (system Ab-Or-An), the phenocrysts plot on the curve that Tuttle and Bowen (1958, p. 135) describe as crystallizing at temperatures for rhyolites and phonolites with a high H_2O content (Fig. 10).

Quartz Phenocrysts

Quartz crystals invariably have equant dimensions, are rounded, and have anhedral to subhedral form. All crystals are embayed and rounded by resorption from formerly euhedral crystals (Figs. 11, 12, and 13). Phenocryst widths vary considerably but predominantly are in the range 0.2 to 0.5 mm. Contacts with the groundmass are commonly very distinct and the embayments are filled with groundmass. Several samples have rims of fine crystals of quartz, apparently a result of reaction and partial resorption (Fig. 13). Crystals having no rims

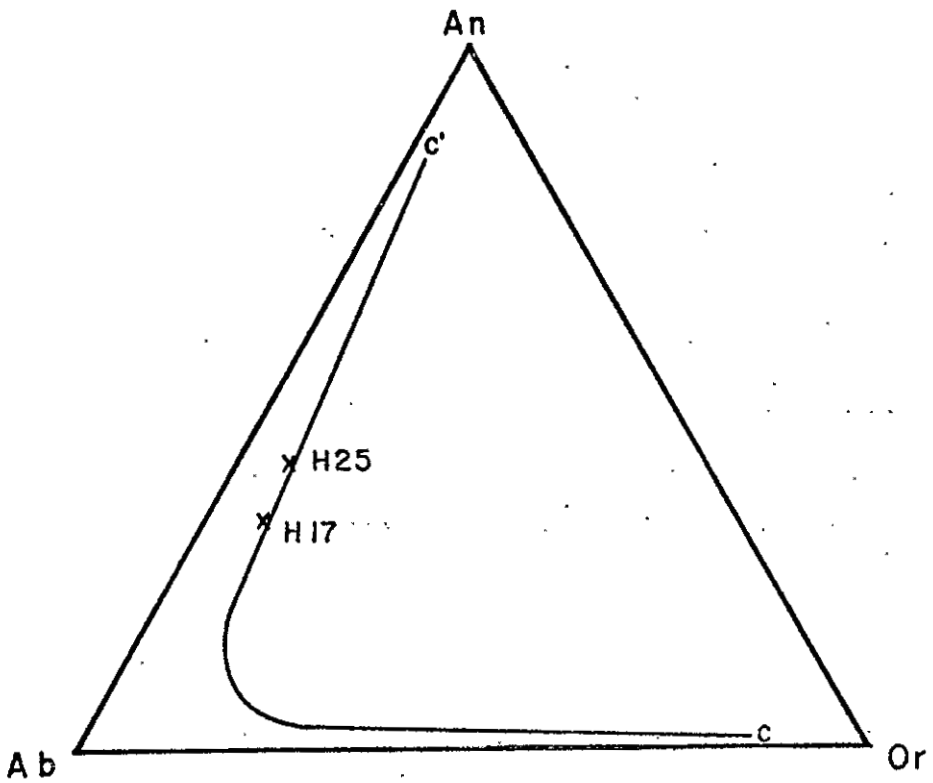

Figure 10. Ternary diagram illustrating solid solution of plagioclase phenocrysts from sample H17 and H25 in the system An - Ab - Or. Line C - C' represents solid solution expected for feldspars crystallizing from rhyolite and phonolites with high water contents (temperature dependant). Curve from Tuttle and Bowen (1958, p. 135).

Figure 11. Highly embayed quartz phenocryst. Crossed nicols; field of view, 2.1 mm wide.

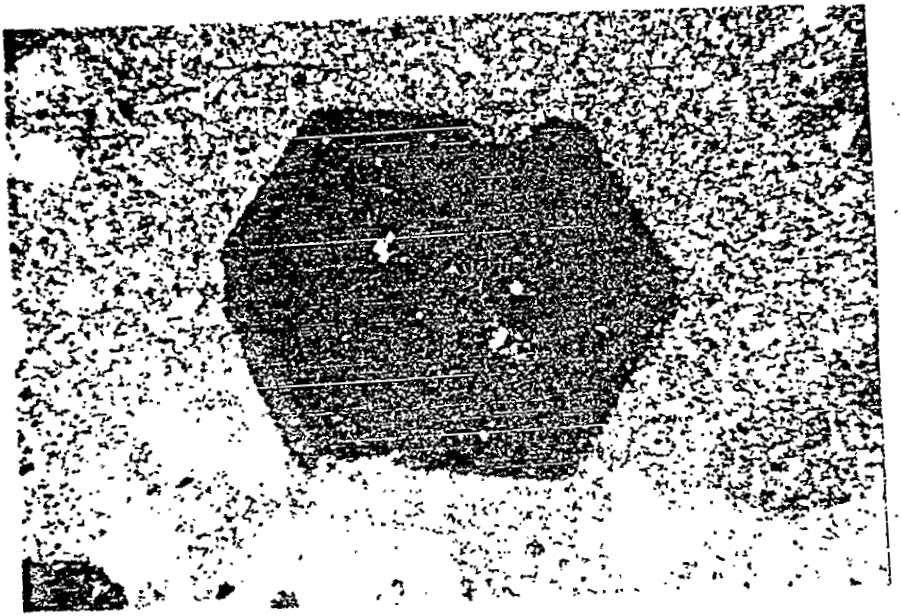

Figure 12. Slightly embayed euhedral quartz phenocrysts (c-crystallographic axis perpendicular to slide). Crossed nicols; field of view, 2.1 mm wide.

Figure 13. Partially resorbed quartz phenocrysts (large white area in lower right and round white area in upper left) with fine-grained quartz rims. Crossed nicols; field of view, 2.1 mm wide.

of fine quartz crystals must be a result of complete dissemination of SiO_2 in the magma after resorption.

The diamond- or square- shaped form of many quartz phenocrysts indicates that they crystallized as beta-quartz (high quartz). The habit of beta-quartz is predominantly hexagonal dipyramidal and prism faces are subordinate. Prism faces are predominant and subhedral or euhedral crystals are elongate if the quartz crystallizes as alpha-quartz (low quartz).

Biotite, Chlorite, and Magnetite Phenocrysts

Biotite, chlorite, and magnetite phenocrysts are discussed together because their genesis may be related, with chlorite and magnetite being alteration products of biotite. Not all magnetite is related to biotite and chlorite; therefore, the following discussion will begin with magnetite not resulting from alteration.

Amount, size, and form of magnetite phenocrysts vary greatly. Crystals appear subhedral and anhedral, generally ranging in diameter from less than 0.01 to 0.75 mm. Larger crystals, up to 2.0 mm in diameter, are found in several samples.

Biotite phenocrysts show reaction relationships such that brown biotite has altered to olive green biotite, opaque oxybiotite, chlorite of various shades of green, and magnetite + sericite + leucoxene. Both green biotite and chlorite appear to be alteration products of brown biotite because brown biotite is seen at the center of some green biotite and chlorite phenocrysts (Fig. 14), never the opposite. Magnetite and sericite are more common around biotite rims than within the crystals (Fig. 15). When sericite is present within a biotite crystal, magnetite is within or adjacent to the sericite (Fig. 16).

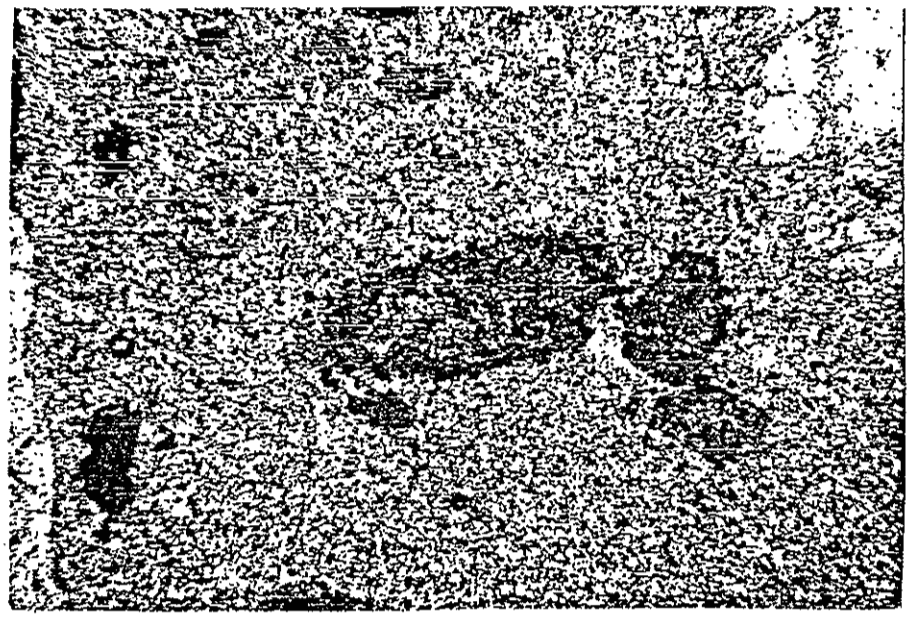

Figure 14. Brown biotite surrounded by green biotite. Black is magnetite. Uncrossed nicols; field of view, 2.1 mm wide.

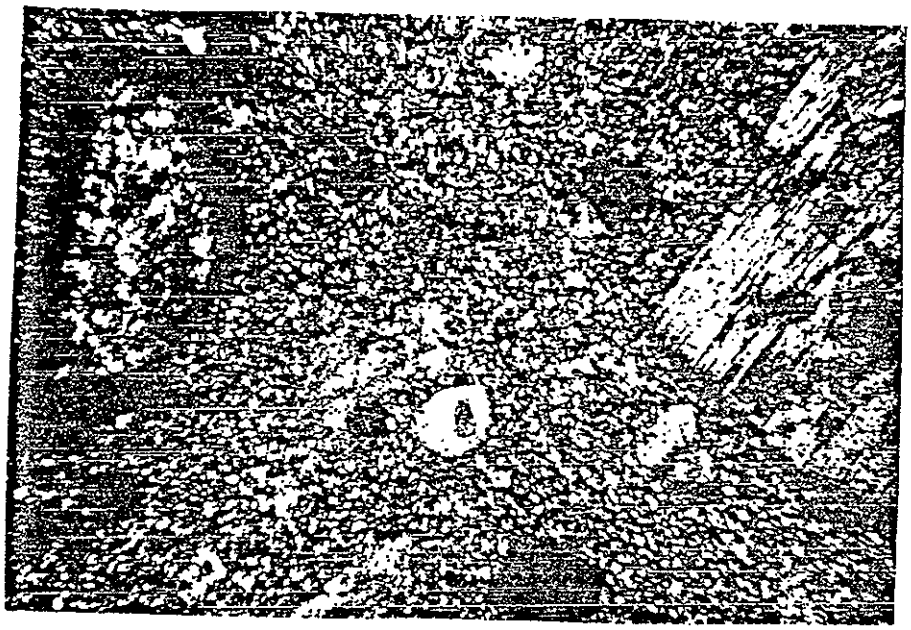

Figure 15. Partially reacted biotite (right) and completely reacted biotite (left). Light colored material in biotite is sericite; black, magnetite. Crossed nicols; field of view, 2.1 mm wide.

Figure 16. Biotite (colored), sericite (light colored), and magnetite (black) showing reaction relationships. Crossed nicols; field of view, 0.75 mm wide.

Sericite has a creamy yellow color due to submicroscopic leucoxene.

All degrees of biotite alteration exist within the sill and commonly within single thin sections. Alteration generally disrupts the crystal structure such that the different varieties of biotite and chlorite are indistinguishable, especially green biotite versus chlorite. Separate phenocrysts within one thin section may range from normal brown biotite to biotite pseudomorphs of sericite + magnetite + leucoxene (Fig. 15). According to Schwartz (1958, p. 176), this non-equilibrium alteration of biotite (i.e., varying degrees of alteration) is not unusual.

Schwartz (1958), in agreement with Winchell and Winchell (1951, p. 376), suggests the following sequence as being typical for biotite alteration, consistent with observations presented above. In the incipient stage of alteration, brown biotite recrystallizes with a change in color to green biotite (very likely deuteric). Next, biotite converts to chlorite. Very fine leucoxene crystallizes from the early release of Ti. Alteration to sericite and magnetite could have occurred at any time. In thin section, it is indeterminable whether the alteration of primary biotite to green biotite and chlorite precedes, follows, or is syngenetic with the alteration to magnetite, sericite, and leucoxene.

The forms of biotite and its pseudomorphs are generally euhedral and subhedral six-sided crystals of tabular habit. The wide dimension is typically 0.2 to 1.0 mm across.

Groundmass

The groundmass is composed of plagioclase, K-feldspar, quartz, ±biotite, and ±magnetite (feldspars distinguished by staining tech-

niques). Finely crystalline magnetite and little or no biotite are visible in the relatively coarse groundmass of samples V19 and V23.

Rough calculations of An for plagioclase in the groundmass of samples H17 and H25 were made using modal data and chemical data from whole rock and phenocryst analyses. Groundmass plagioclase for sample H17 has An near 0; for sample H25, approximately 18.

Dissolution Voids

Voids are found in all thin sections. They occupy less than 2 percent of the rock volume (except for sample V23 which is approximately 4 percent void). It is obvious from thin section examination that these voids are caused by dissolution of crystalline phenocrysts and groundmass and are not simple vesicles (Figs. 17, 18, and 19). Otherwise, the voids would be found only in the groundmass. Percentage and distribution of these voids, which will be referred to as dissolution voids, are inconsistent and no correlation can be made to sample location.

Dissolution voids are in groundmass and in all types of phenocrysts except quartz. Only sample V23 contains dissolution voids in quartz phenocrysts. In most thin sections, voids are more common in plagioclase and biotite phenocrysts than in the groundmass. Crystalline material adjacent to voids does not appear to be altered or disrupted.

Samples V23 and V24 are unusual for three reasons. First, dissolution voids are most abundant in these two samples. Second, very little or no biotite or magnetite is visible, and it is unclear whether these minerals were leached out during formation of the voids or whether the samples never contained them prior to leaching. Along the edges of some dissolution voids, a very irregular opaque "iron

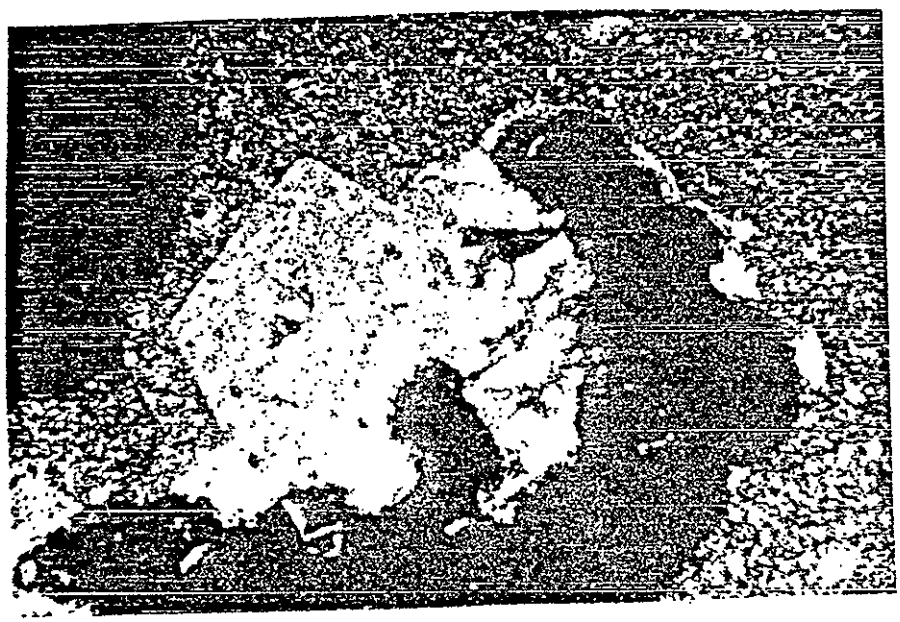

Figure 17. Dissolution void (black) in a plagioclase phenocryst and groundmass. Crossed nicols; field of view, 2.1 mm wide.

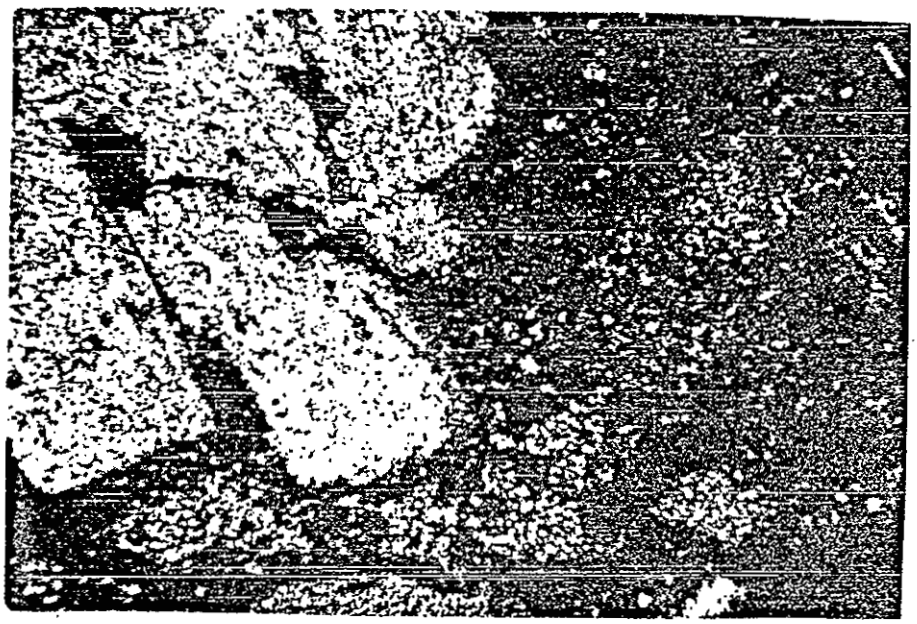

Figure 18. Dissolution voids (larger black areas) in a plagioclase phenocryst, a biotite phenocryst, and groundmass. Crossed nicols; field of view, 2.1 mm wide.

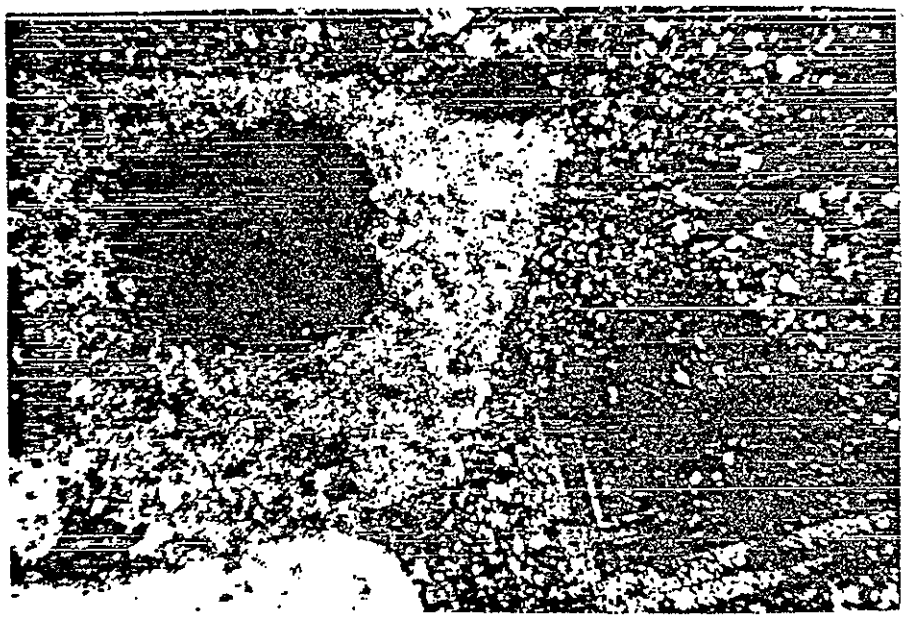

Figure 19. Dissolution void (black) in core of plagioclase phenocryst. Crossed nicols; field of view, 2.1 mm wide.

oxide" is seen, possibly resulting from reprecipitation of leached iron. Third, some of the dissolution voids are partially filled with quartz which grew radially from the outside toward the center, leaving a void in the middle. Under a petrographic microscope with crossed nicols, these radial growths produce an "isogyre" effect around the void (Fig. 20), a result of radial orientation of quartz's c-crystallographic axis.

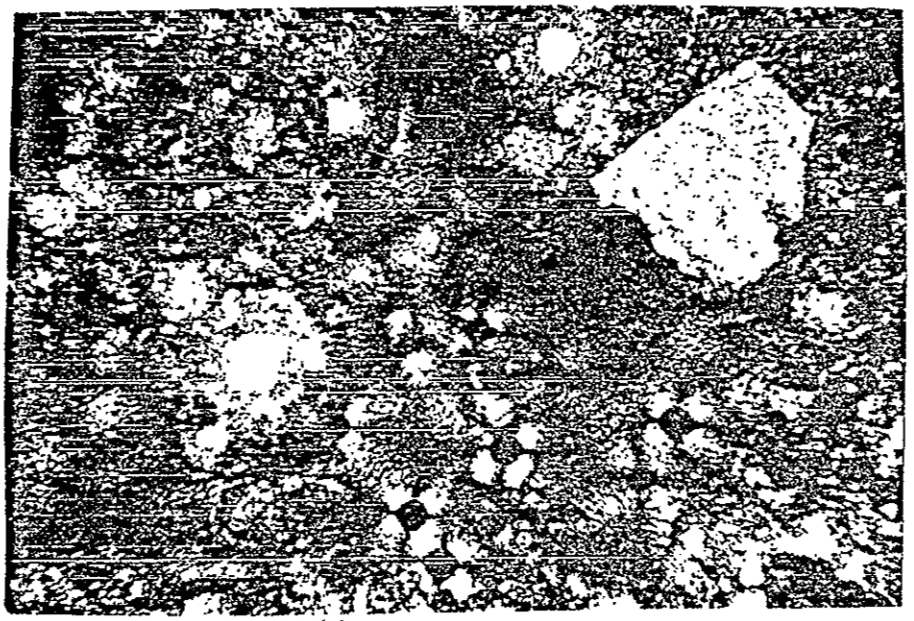

Figure 20. Dissolution voids filled with radially oriented quartz causing the "isogyre"effect (round voids at center of quartz growth). Crossed nicols; field of view, 2.1 mm wide.

CRYSTALLIZATION AND ALTERATION

Chemical and petrologic information used in conjunction with experimental data are used to develop a coherent and consistent crystallization and alteration model for the Palisades sill. The observations presented above are the basis for this model.

Intrusion

Relation between Magma and Phenocrysts

Quartz, biotite, and plagioclase phenocrysts apparently crystallized from the magma in a deep chamber before intrusion to the present position of the sill. Modal data (Table 4) indicate that the amount of biotite and plagioclase phenocrysts for different parts of the magma chamber was constant.

The percentage of quartz phenocrysts was probably constant for all of the magma before embayment. In thin section, 10 to 11 percent modal quartz is found when the phenocrysts are least embayed and still display crystal faces. Samples with extremely embayed and small quartz phenocrysts contain less than 6 percent modal quartz phenocrysts. Intermediate degrees of embayment and intermediate quantities of modal quartz also exist. Before intrusion, all parts of the magma probably contained 10 to 12 percent euhedral quartz crystals.

Crystal settling and floating can be ruled out, either before or after intrusion, based on phenocryst distribution, chemical data, and comparison with experimental and theoretical data. Table 4 shows that distribution of phenocrysts throughout the sill is constant,

indicating that crystal settling and floating did not occur during crystallization of phenocrysts and/or groundmass. As a result, equilibrium crystallization is the dominant process. No correlation can be drawn between magnetite ($\approx$ 5.2) and position in the sill; therefore, crystal settling for other minerals would be very unlikely (Shaw, 1965, p. 128). For magma as viscous as the Palisades sill magma was during intrusion (approaching the system Ab-Or-SiO_2-H_2O), Bartlett (1969) has demonstrated that phenocrysts as small as those in the sill could not have settled. They would follow convective or forced flow without "slippage" of the crystals in the fluid.

No reasons exist to suspect any type of metasomatism or contamination from either country rock or mixing with other magmas. Absence of xenoliths, apparent constant abundance and composition of phenocrysts and groundmass, and predictability of sample chemistry are evidence for a simple model involving equilibrium crystallization.

Effects of Pressure Change during Intrusion

The minimum depth of intrusion estimated from maps and cross sections of Robinson and others (1964) is probably 1,5000 to 3,000 m. The approximate lithostatic pressure for the latter depth would be 900 bars, assuming a density of 2.3 gm/cc for overlying material (Nash and Wilkinson, 1970, p. 256). The magma clearly underwent a substantial pressure drop on intrusion, and pressure sensitive reactions of phenocrysts and magma are likely to have occurred.

Partial resorption of quartz is the most obvious effect of lowering pressure, an effect not uncommon in volcanic rocks. Resorption of quartz with pressure decrease is dependent on water content of the magma. If the magma is dry or less than H_2O saturated, the phase

boundary of a PT diagram for quartz has a positive slope (Boyd and England, 1960, p. 752) so that a drop in total pressure at a constant temperature could cause quartz to resorb (Fig. 21). If the magma is water saturated, a drop in pressure will enhance crystallization.

Fyfe (1970) suggests that most "granitic" magmas are water-undersaturated, and it is generally accepted that more mafic igneous rocks are very dry. Other reasons to suspect that the Palisades sill magma was water-undersaturated are as follows. First, P_{H_2O} is buffered by reactions such as

$$KFe_{2-3}(AlSi_3O_{10})(OH)_2(\text{biotite}) \rightleftharpoons$$
$$KAlSi_3O_8(\text{K-feldspar}) + Fe_3O_4(\text{magnetite}) + H_2O$$

(Fyfe, 1970, p. 205) and

$$2KFe_{2-3}(AlSi_3O_{10})(OH)_2(\text{biotite}) + 2Al_2O_3 + H_2O \rightleftharpoons$$
$$K_2Al_4(OH)_4Si_6Al_2O_{20}(\text{sericite}) + Fe_3O_4(\text{magnetite}).$$

The mineralogic relationships for the latter reaction are observed in the Palisades sill. Second, if P_{H_2O} is high it will lower the phase field of quartz so that it will near the K-feldspar phase boundary (Eggler, 1974, and Piwinskii and Wyllie, 1970). Since no K-feldspar phenocrysts are found in the sill, it is most likely that P_{H_2O} was not equal to P_{total} so that the quartz phase boundary was at a higher temperature relative to the K-feldspar boundary. Third, the magma must have been H_2O undersaturated before intrusion. Otherwise, the magma would have reached saturation, "second boiling", on intrusion and quartz would not have been resorbed (Burnham and Jahns, 1962).

One other possibility exists for the resorption of quartz. An increase in P_{H_2O} could lower the quartz melting temperature such that quartz phenocrysts could resorb, but there is no reason to suspect

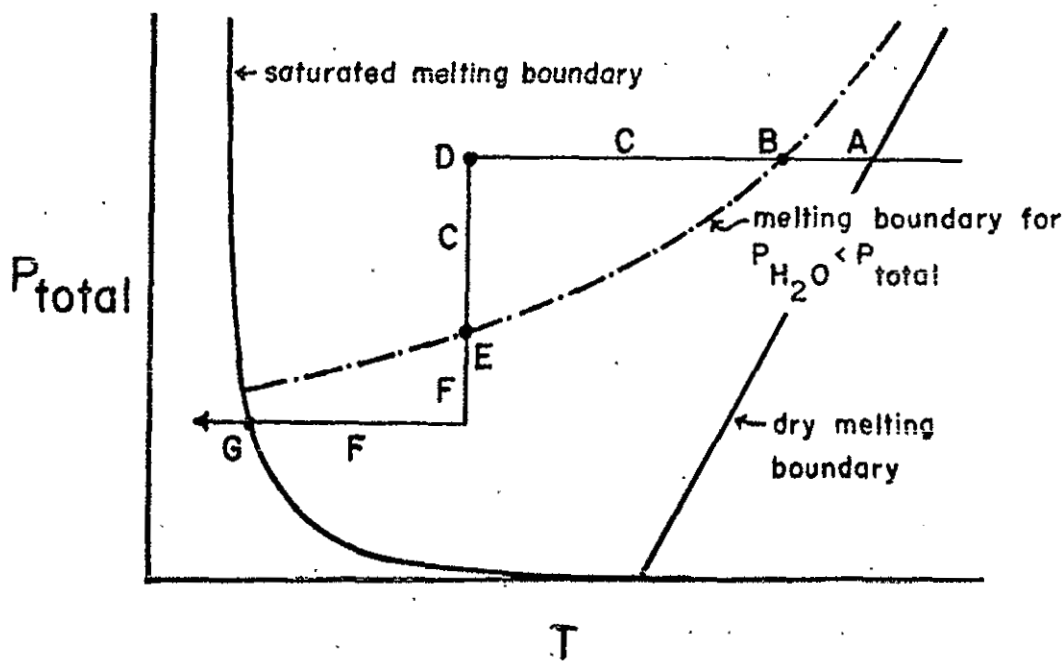

Figure 21. Schematic pressure-temperature diagram showing possible quartz crystallization - resorption history in the Palisades sill assuming instantaneous intrusion and P_{H_2O} less than P_{total} (after Brown, 1970, p. 356, and Harris and others, 1970, p. 191). Dashed line is a quartz melting boundary for a constant P_{H_2O} where P_{H_2O} is less than P_{total}.

Field A - liquid
Point B - quartz begins to crystallize
Field C - quartz crystallizes
Point D - intrusion of magma
Point E - Quartz begins to melt
Field F - quartz resorbs
Point G - quartz crystallization resumes

such a change. If water were added, the H_2O buffers described above would have absorbed much of it. It is unlikely that added water would be homogenously mixed throughout the sill as it would have had to be since quartz phenocrysts in all samples show resorption.

Different degrees of quartz resorption arerelated to silica mobility. Least affected crystals have a narrow rim of extremely fine grained quartz, clearly a result of reaction and resorption (Fig. 13) without effective mixing of resorbed SiO_2 and magma. The most embayed crystals never have a rim (Fig. 11), indicating that the silica was more mobile. That is, more SiO_2 was able to react and disperse into the liquid due to local variations in viscosity.

It is uncertain whether plagioclase phenocrysts were also affected by the pressure drop on intrusion. They are generally subhedral and edges are slightly "corroded." This slight resorption phenomenon is possibly due to the pressure drop with plagioclase less affected than quartz because of its higher temperature and pressure stability field.

Because biotite is a hydrous mineral, its phase boundary has the opposite slope from that of plagioclase and quartz; therefore, biotite should be more stable upon lowering of total pressure.

Chill Zone, Magma Convection, and Temperature Distribution

It is not clear whether the Palisades sill has a chill zone. No definitive evidence is available, texturally or chemically. All groundmass is sufficiently fine grained that a chill zone may not be significantly finer. Chemically, the sill is homogeneous enough such that a chill zone can not be distinguished.

A possible chill zone is found at the lower contact. Of samples from which thin sections were made, the closest sample to the lower

contact in the H-profile, H1, and the closest two samples in the V-profile, V1 and V4, have the finest groundmass. Samples H1 and V1 are less than 1.0 m from the contact; sample V4, approximately 30.5 m from the contact. Another observation was made with regard to sample H1. The thin section for this sample contains several kinked chlorite crystals, possibly indicative of a solidifying groundmass during forceful intrusion.

Samples at the upper contact show no evidence of being chilled, but textural features indicate that the highest 30 to 90 m of the V-profile crystallized before the majority of the magma. Evidence for this is the coarse groundmass in sample V23, a coarser than average groundmass in V19, and the concentration and nature of dissolution voids in their vicinity. The coarser groundmass of samples V23 and V19 is interpreted as a result of higher fluid content during crystallization. It is presumed that water content would increase in the last stages of crystallization and would migrate to the highest level of magma remaining in the sill. If the material above sample V23 were crystalline, fluid would collect in the vicinity of V23 and thus cause the development of larger crystals. Sample V19 probably crystallized at a later time after the samples above had completed crystallization, again creating a cap under which fluid could accumulate.

Dissolution voids in samples V23 and V24 are numerous, especially V23, in which dissolution voids occupy 3 to 4 percent of the rock. This may be taken as a result of concentration of the dissolving volatiles below a well crystallized and cooler capping material. The "corrosive" volatiles apparently concentrated near samples V23 and V24 and became oversaturated to the point that quartz re-precipi-

tated in some of the dissolution voids.

Magma convection is a process which probably occurred after intrusion and prior to crystallization, keeping the temperature gradient to a minimum. Convection also confuses interpretation of chemical and mineralogic distribution on intrusion. Bartlett (1969, p. 1069-1071) has demonstrated that a granitic magma is expected to have natural convection for a sill the thickness of the Palisades sill (Fig. 22). The viscosity of the Palisades sill on intrusion should be roughly the same viscosity as granite magma since the liquid had a "granitic" composition after the phenocrysts crystallized. Shaw (1965) predicts that granitic melts will have viscosities between 10^8 and 10^5 poises with magmas containing as much as 50 percent phenocrysts.

An order-of-magnitude approximation for the crystallization time for the Palisades sill is 600 to 1400 years (Turner, 1968, p. 20; Carmichael, 1974, p. 446). Although the rate of convection is unknown, it is certainly possible for the magma to have overturned numerous times. Individual convection cells are generally hexagonal in form with width approximately equal to height (thickness of the sill) in which the magma flows up the center of the cell and down the sides (Bartlett, 1969, p. 1069).

Convective overturn kept temperature differences in the cell relatively small. If the temperature gradient becomes large either by cooling of the magma through the ceiling or through both the ceiling and the floor, density inversion in part of the magma will cause convective overturn, decreasing the temperature gradient (Bartlett, 1969).

Convection tends to promote equilibrium crystallization. If no

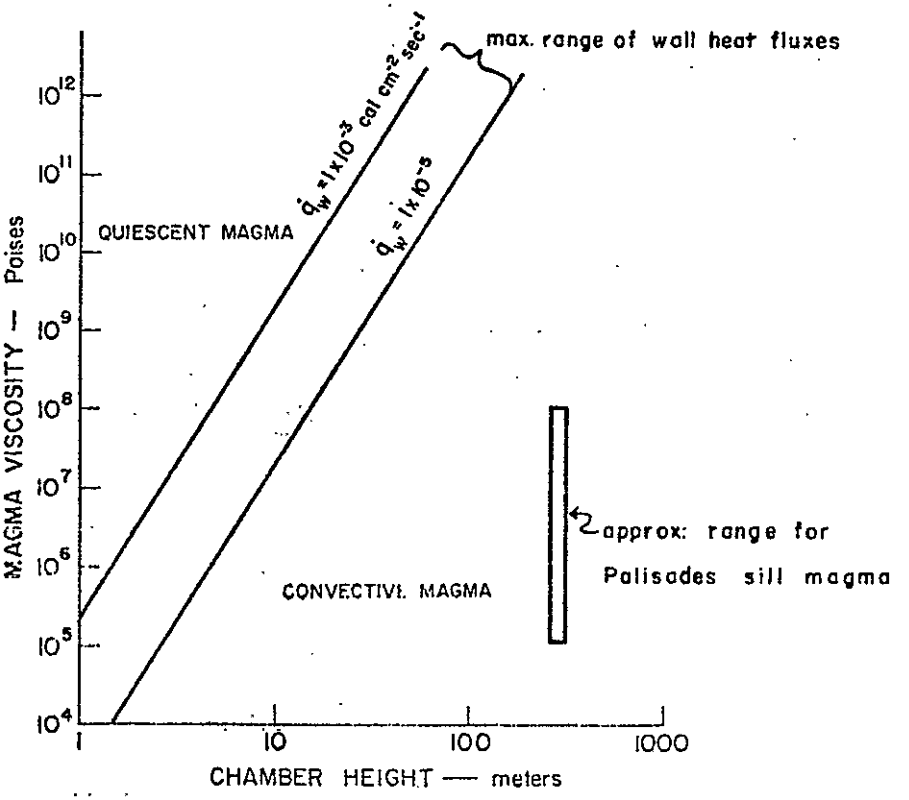

Figure 22. Stability range of the Palisades sill magma after intrusion based on magma convection stability limits from Bartlett (1969, p. 1071).

convection occurred, two factors should be observable. First, textures resulting from different lengths of time for crystallization should be systematic in relation to "stratigraphic" position in the sill. Variations in crystal size of the groundmass and abundance of dissolution voids should show some systematic pattern from top down, neither of which can be demonstrated. Second, chemical and mineralogical variations should be more systematic in relation to "stratigraphic" position as a result of fractional crystallization, a process which would be more likely if the magma crystallized with a large temperature gradient. There is no evidence that in situ fractional crystallization and its subsequent elemental differentiation occurred either from the top down, from the bottom up, or toward the center. Oxides do show significant variation but not in a "stratigraphic" pattern.

Deuteric Alteration

Two possible types of deuteric or late magmatic alteration exist. One is the alteration of biotite and plagioclase phenocrysts. The other is the dissolution of groundmass and phenocrysts.

Phenocryst Alteration

It is unclear how much of the biotite and plagioclase alteration is deuteric. Some of the biotite reaction relationships and plagioclase phenocrysts clouding and disruption of crystallinity may be due to deuteric alteration. Plagioclase alteration could be caused by pressure changes during intrusion, by slight P_{H_2O} variations in the magma, or by deuteric reactions which cannot be defined optically. Many authors consider the reactions, biotite to chlorite and plagioclase to sericite, deuteric alteration.

Since biotite has been altered to a large degree, the author

considers only biotite to chlorite and brown biotite to green biotite as deuteric effects. It has been demonstrated that the biotite to sericite + magnetite reaction may be H_2O buffered and was probably a continuous process after crystallization of biotite phenocrysts.

Phenocryst and Groundmass Dissolution

Dissolution to produce voids is a deuteric process since the groundmass was crystalline, since the source of the corrosive fluid was probably internal, and since the minerals were probably at near-liquidus temperature when dissolved. Only two references of dissolution of crystals in igneous rocks could be found. Salotti and Matthews (1969) reported quartz leaching from wall zone graphic granite in a zoned pegmatite. Barker and Burmester (1970) reported complete removal of quartz and albite with decomposition of biotite, leaving only microcline and a red iron stain in two outcrops of a hypabyssal rhyolite porphyry. They attribute this leaching to contact of the samples with a highly alkaline brine (pH greater than 9) long after crystallization.

Dissolution probably occurred at near-solidus temperature with removal of material in a low viscosity and highly corrosive H_2O rich medium. Near-solidus temperature was necessary so that the minerals dissolved were relatively near their instability fields and the concentration and amount of the corrosive constituent was not high.

Experimental results of Wyllie and Tuttle (1961 and 1964) on the effects of SO_3, P_2O_5, HCl, Li_2O, NH_3, and HF in addition to H_2O on melting temperatures of granite demonstrate that HF and Li_2O are the most likely corrosive volatiles that produced dissolution of plagioclase in preference to quartz, the relationship observed in the

Palisades sill. These studies show that HF and Li_2O in H_2O lower the stability field of plagioclase relative to the quartz field. Wyllie and Tuttle (1961, p. 141) state, "The feldspar is less stable in the presence of HF solutions than in the presence of H_2O, as would be expected, and the quartz appears to be more stable." Although these studies involve melting of minerals, lowering of the feldspar stability field relative to the quartz field may be the explanation why plagioclase is more susceptible to dissolution than quartz. Pure H_2O would not be responsible for lowering the plagioclase stability field relative to the quartz field as is shown from phase diagrams of "granitic" rocks (Tuttle and Bowen, 1958; Piwinskii, 1968).

The amount of HF or Li_2O required to lower significantly the stability fields of plagioclase relative to quartz is not prohibitively high. According to Wyllie and Tuttle (1964, p. 937), to lower the temperature of beginning of melting only requires "a few tenths of 1 weight percent (of HF or Li_2O) if a smaller proportion of total volatile components is employed" than they used in experimentation.

Comparison with Experimental Results

Figure 23 is a pressure-temperature diagram of melting relations in natural rocks ($P_{H_2O} = P_{total}$) that should be a best approximation for the Palisades sill based on mean oxide values, phenocryst mineralogy, and experimental data from Piwinskii (1968) and Piwinskii and Wyllie (1970). Figure 23 is a synthesis of PT projections of phase boundaries for eight igneous rocks including granite (2), granodiorite (3), quartz monzonite (2), and tonalite (1). Since the chemistry and mineralogy of none of these samples can be directly correlated with Palisades sill samples, the following reasoning has been used to

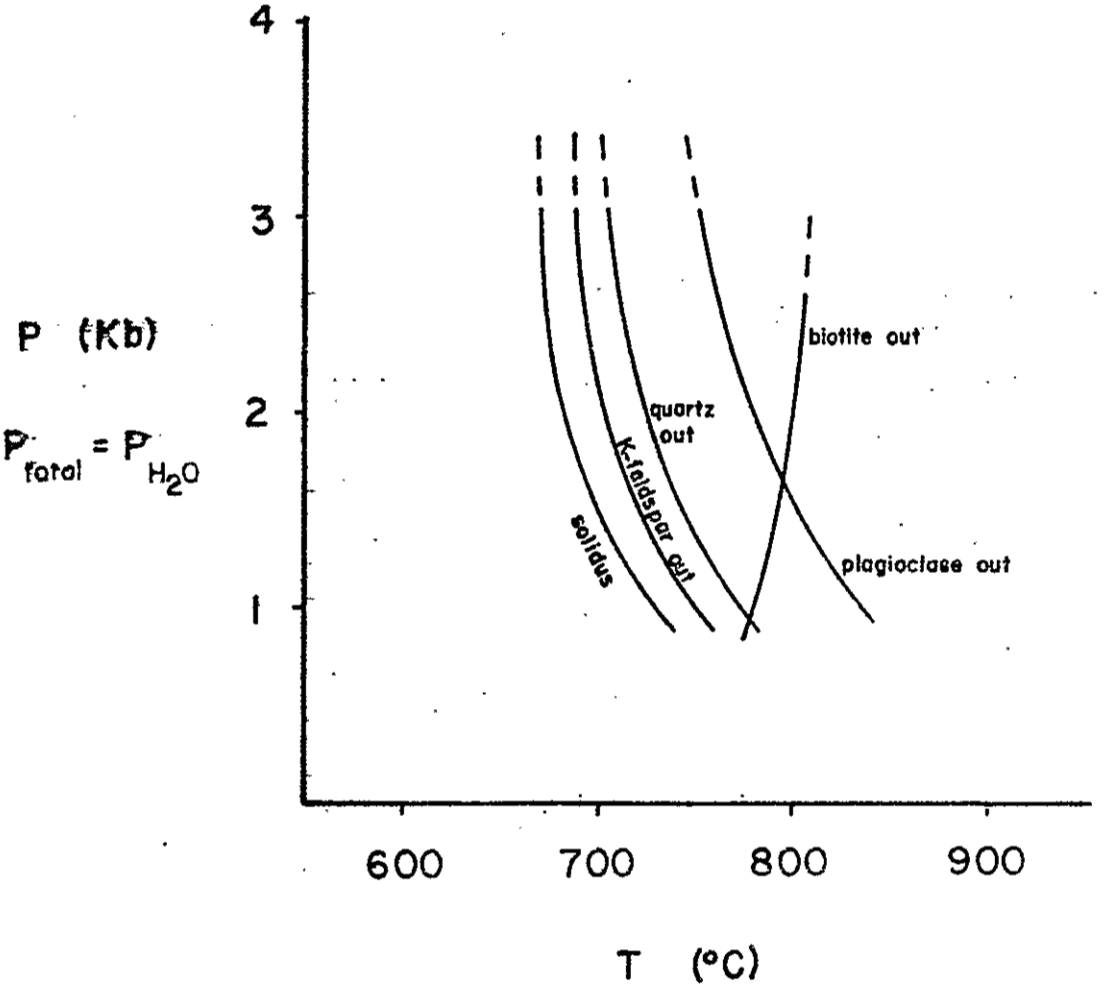

Figure 23. Estimated phase boundaries predicted for the Palisades sill assuming $P_{H_2O} = P_{total}$ (after Piwinskii, 1968; Piwinskii and Wyllie, 1970).

construct the diagram: 1) The plagioclase phase boundary is based on rocks not containing hornblende. When hornblende is present, the plagioclase phase boundary is approximately 100° C higher at comparable pressures. Whole rock CaO:Na_2O ratios have little affect on the boundary. 2) The biotite phase boundary is based on the only non-granitic sample that contains no hornblende. Granites used in their studies have extremely low Fe_2O_3* and MgO, and when hornblende is present in other samples, the temperature of the biotite phase boundary is relatively high.

The experimental work demonstrated above (Fig. 23) agrees well with the crystallization sequence determined petrographically for the Palisades sill. At pressures above 1.5 Kb, biotite is the first mineral to crystallize, followed by plagioclase and quartz. Intrusion of the sill occurred before the temperature reached the K-feldspar phase boundary. The pressure required needs to be above 1.5 Kb, deeper than 5.5 Km, but no upper limit of pressure can be made. These assumptions are based on $P_{H_2O} = P_{total}$, and although they are not strictly correct, are probably reasonable estimates.

System Q-Ab-An-Or-H_2O (saturated) as described by Winkler (1974) and Winkler and others (1975) also demonstrates that the Palisades sill magma underwent equilibrium crystallization and crystallization in the same mineralogic sequence as described above. Figure 24 is a plot of two samples using whole-rock normative data. These samples were chosen to represent extremes in composition. Most other samples plot in or near the space between these two points. As shown from the position of these points with respect to phase fields (assuming they represent the composition of the melt), plagioclase is the first min-

eral expected to crystallize. As plagioclase crystallizes and temperature lowers, the composition of the magma will move away from the point along a nearly straight line which intersects that point and a point on the Ab-An edge which is determined by the composition of the plagioclase crystals. When the magma composition reaches the surface E_1-E_2-E_3, quartz will begin to crystallize. Magma composition will move along or near the plagioclase-quartz boundary toward the cotectic line, P-E_5, at which temperature K-feldspar begins to crystallize. Since the temperature of crystallization at point E_5 is approximately 50° C higher than at point P (Winkler and others, 1975, p. 267), the liquid composition will move along the cotectic line toward P until the remaining magma is crystallized.

System Ab-An-Q-H_2O is useful in demonstrating equilibrium crystallization of plagioclase. Figure 25 gives the plot in the system Ab-An-Q-H_2O (saturated) of 20 samples using modal data. As stated previously, plagioclase phenocrysts of samples H17 and H25 have an An-content of approximately 35 and 44, respectively; An-content of plagioclase in the groundmass, nearly 0 for H17 and 18 for H25. Whole-rock CaO composition is low for sample H17 and is high for sample H25 compared with all other samples. These data are consistent with equilibrium crystallization of plagioclase as shown in Figure 25.

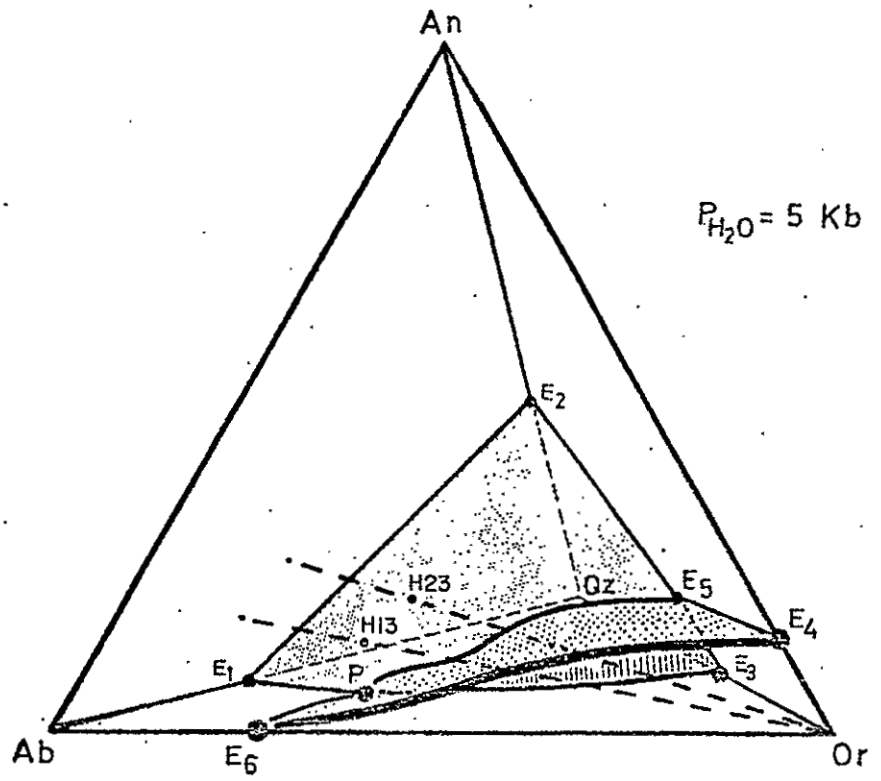

Figure 24. Plot of samples H13 and H23 using normative date on system An - Ab - Or - Q ($P_{H_2O} = P_{total}$) (Winkler and others, 1975, p. 246).

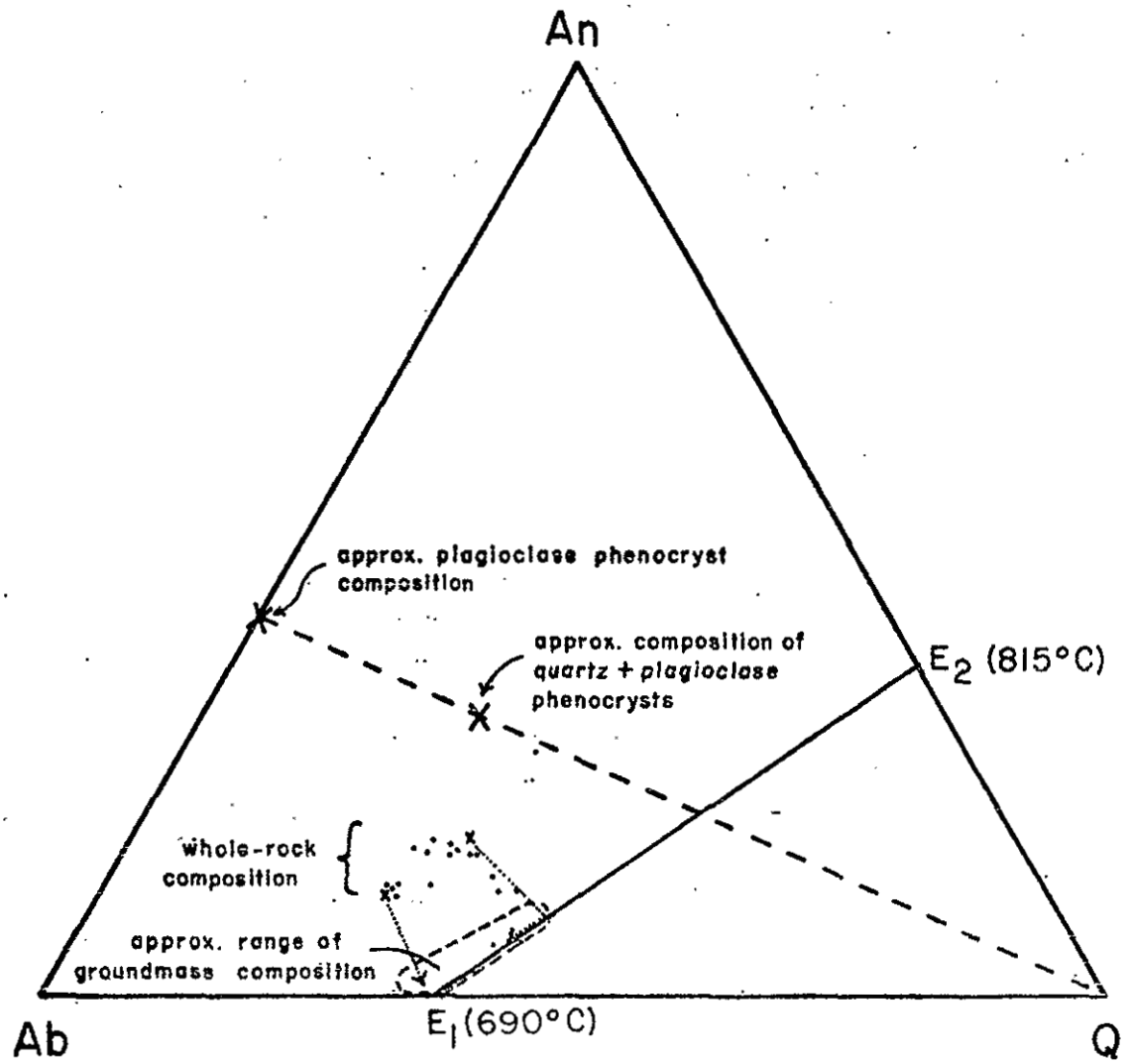

Figure 25. Relationships of sample whole rock composition (·) (from normative data) with approximate phenocryst and groundmass composition in the system An-Ab-Q ($P_{H_2O} = P_{total}$) (after Winkler and others, 1975). Small x - whole rock composition of samples H13 and H23 (see Fig. 24). Dotted line - approximate magma composition as plagioclase and quartz phenocrysts crystallized for sample H13 and H23.

MODE OF EMPLACEMENT

A model for the mode of intrusion, emplacement, and possible convective history before final crystallization cannot be precisely defined. Chemical data are far more complete and accurate as well as show more variation than does petrographic information; therefore, they will be the basis for the model. To make such a model, the topographic nature of the collection profiles for the two profiles is compared with chemical data both between the two profiles and within the V-profile.

Table 1 and comparison of Figures 4, 5, and 8 demonstrate that no "stratigraphic" correlation of chemistry can be made between the two profiles, ruling out a strictly horizontally layered intrusive model. Furthermore, V-profile, which has a limited areal extent (less than 450 m) shows less oxide variation than H-profile, which has an areal extent of approximately 2,000 m (Table 1). The magma must have intruded in isochemical and isomineralogic "fronts" (isopleths) that were apparently altered and mixed by convection before complete crystallization. Figure 26 shows the cyclic chemical pattern for H-profile using two highly variable elements, CaO and Rb. Several large scale and corresponding cycles are shown for both elements. Figure 27 is the author's conception of the intrusion and chemical distribution of the sill before convection. The isopleths could be a result of continuous change in the chemistry of the incoming magma or

Figure 26. Cyclic CaO and Rb variation vs sample location in the H-profile. Sample location projected to a vertical plane containing dip of sill's contacts.

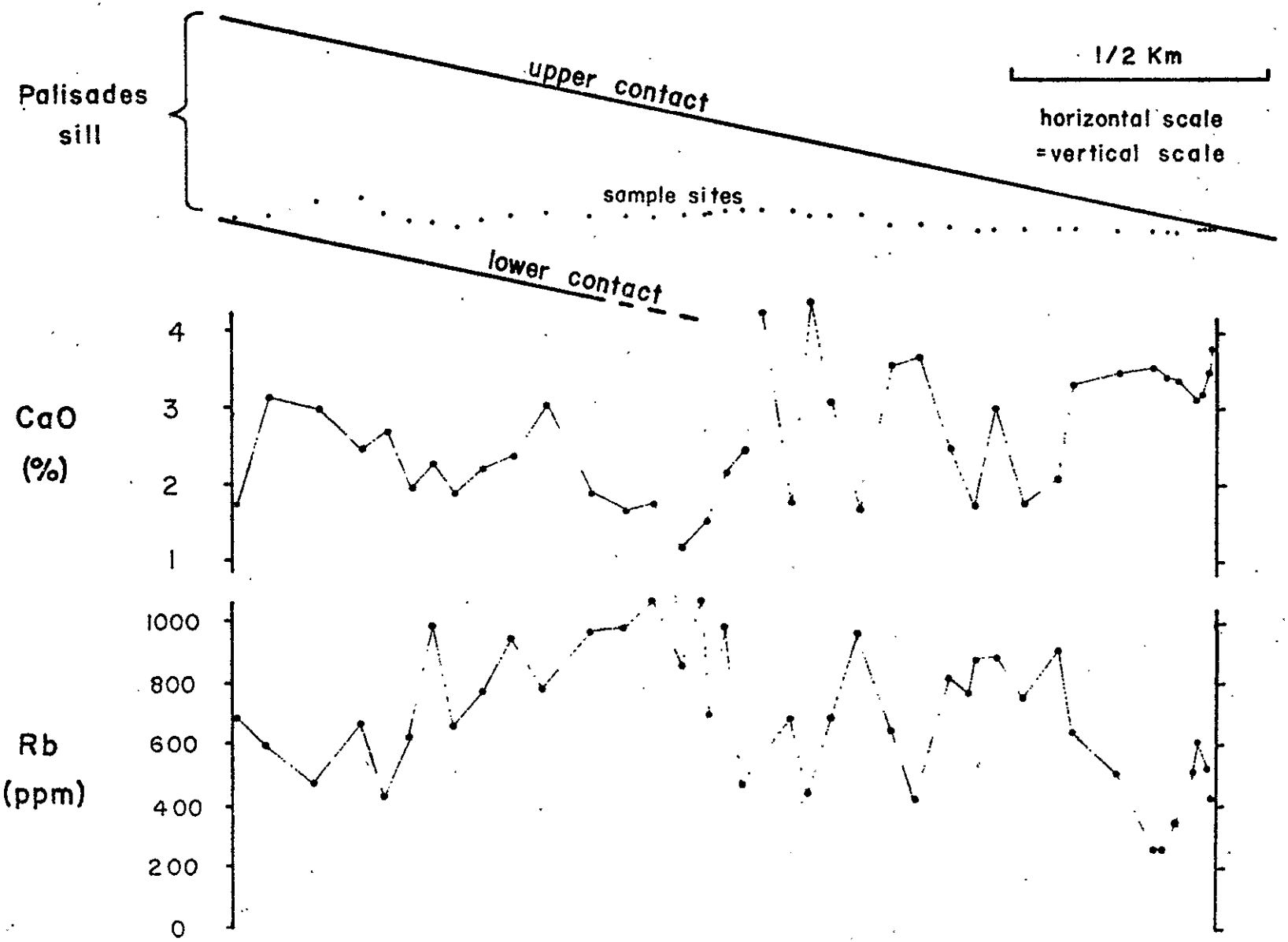
Palisades sill
upper contact
lower contact
sample sites
1/2 Km
horizontal scale
=vertical scale
CaO (%)
4
3
2
1
Rb (ppm)
1000
800
600
400
200
0

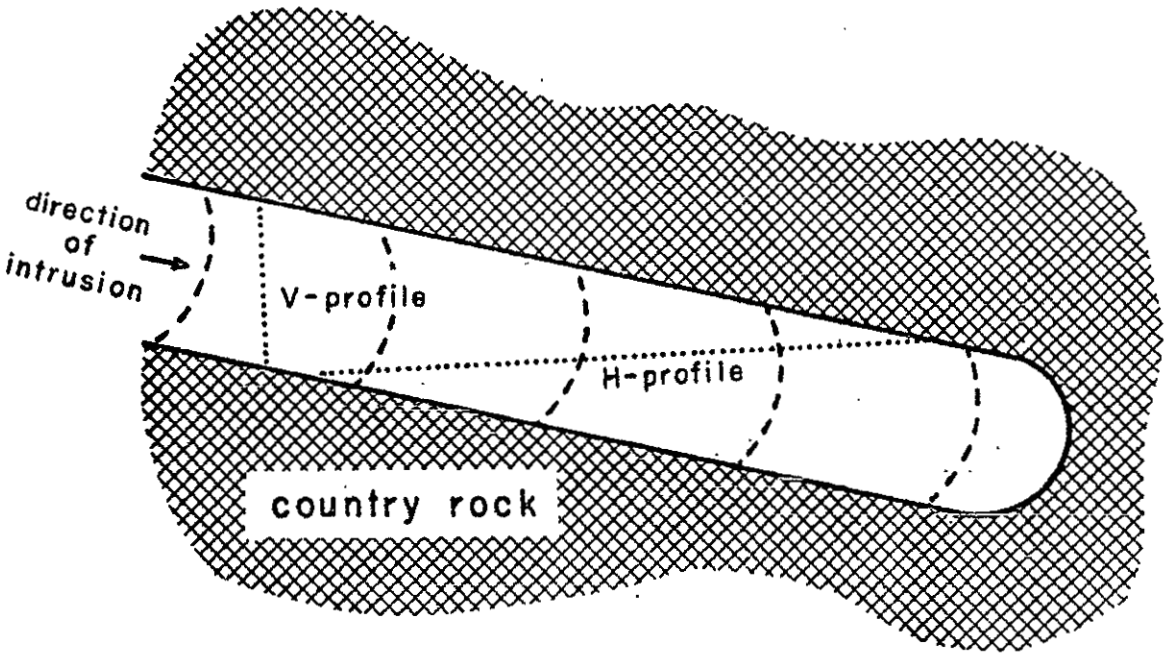

Figure 27. Schematic cross section of the Palisades sill showing element distribution prior to convection. Dashed lines - isochemical and isomineralogic "fronts".

a result of "pulses" of different chemical composition. As magma intruded, previously intruded magma was pushed in front. The exact orientation and direction of movement of the isopleths cannot be determined.

During the time interval when magma was being tapped from the chamber, the following two possibilities can explain the cyclic compositional changes:

1) The variation could be caused by differential ionic diffusion as a result of a temperature gradient in the top of the magma chamber with the differentiated part of the magma being removed in "pulses" represented by a complete cycle. Although no experimental evidence is available, it may be reasonable to postulate that Rb, Na, and Ca (the most variable elements in concentration) diffused in the magma relative to a temperature gradient near the top of the magma chamber. Eichelberger (1975) demonstrates that a single magma body can have coexisting felsic and intermediate composition segments with a mixed zone between. Since Na and Rb concentrations are the antithesis of Ca concentration in samples from the Palisades sill, Na and Rb may have been enriched at a higher level than Ca or vice versa. Each compositional cycle shown in Figure 26 represents one pulse in which both Na + Rb enriched magma and Ca enriched magma, both near the top of the chamber, were removed (Fig. 28). A period of time must have elapsed before the next pulse of magma was intruded, during which diffusion again produced a concentration gradient.

2) Another explanation involves partial melting at a constant depth from a subducting plate which moved at an inconsistent rate with magma being continually removed and intruded. Lipman and others (1972) have

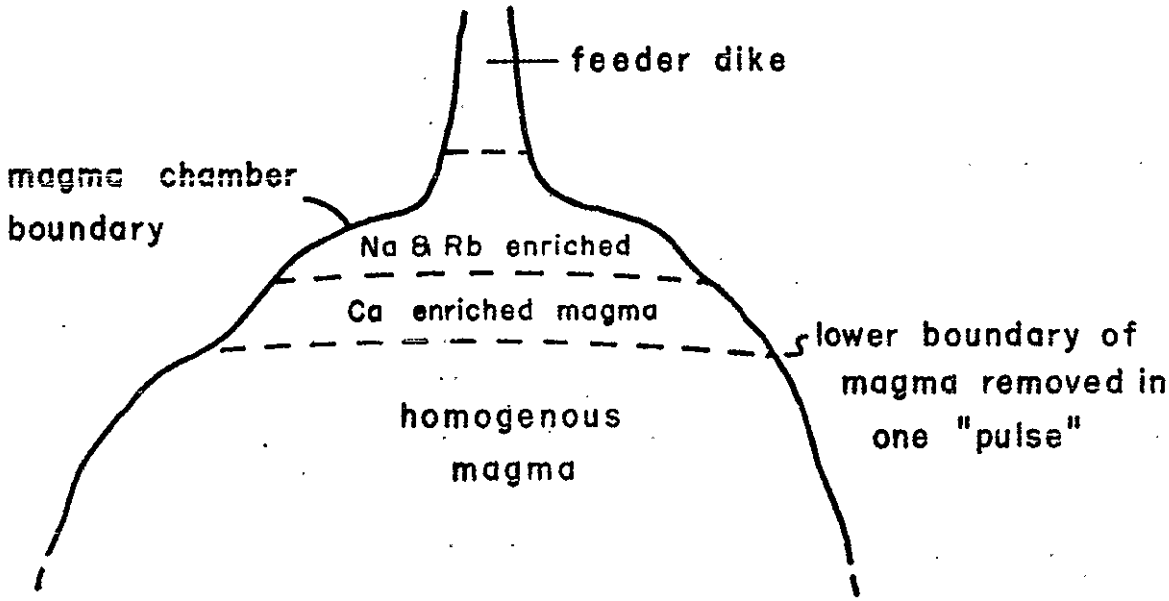

Figure 28. Schematic diagram demonstrating possible segregation in magma chamber immediately before intrusion of one pulse.

proposed subduction of an imbricate zone during early and middle Cenozoic giving rise to predominantly intermediate composition volcanic and intrusive rocks. The Palisades sill may be due to this magmatic activity since the postulated subduction zone correlates both temporally and spatially (Fig. 29). Additional evidence for the Palisades sill being related to the subduction zone is that the magma source depth of 280 km approximated from Figure 29 is close to the depth calculated using chemical data. Mean SiO_2 and K_2O values for the Palisades sill in connection with data of Lipman and others (1972) for the nearby Spanish Peaks igneous center is used to calculate the magma source depth, found to be approximately 250 km. If the subducted plate were almost stationary for a period of time, partial melting in a limited area would produce a magma with a high Na + Rb:Ca ratio first, changing to a lower ratio with time. If the plate were to move far enough to bring fresh material into the zone of melting and slow down or stop again, the melting sequence would occur for a second time. The Palisades sill magma could be a result of partial melting of different parts of an inconsistently moving plate.

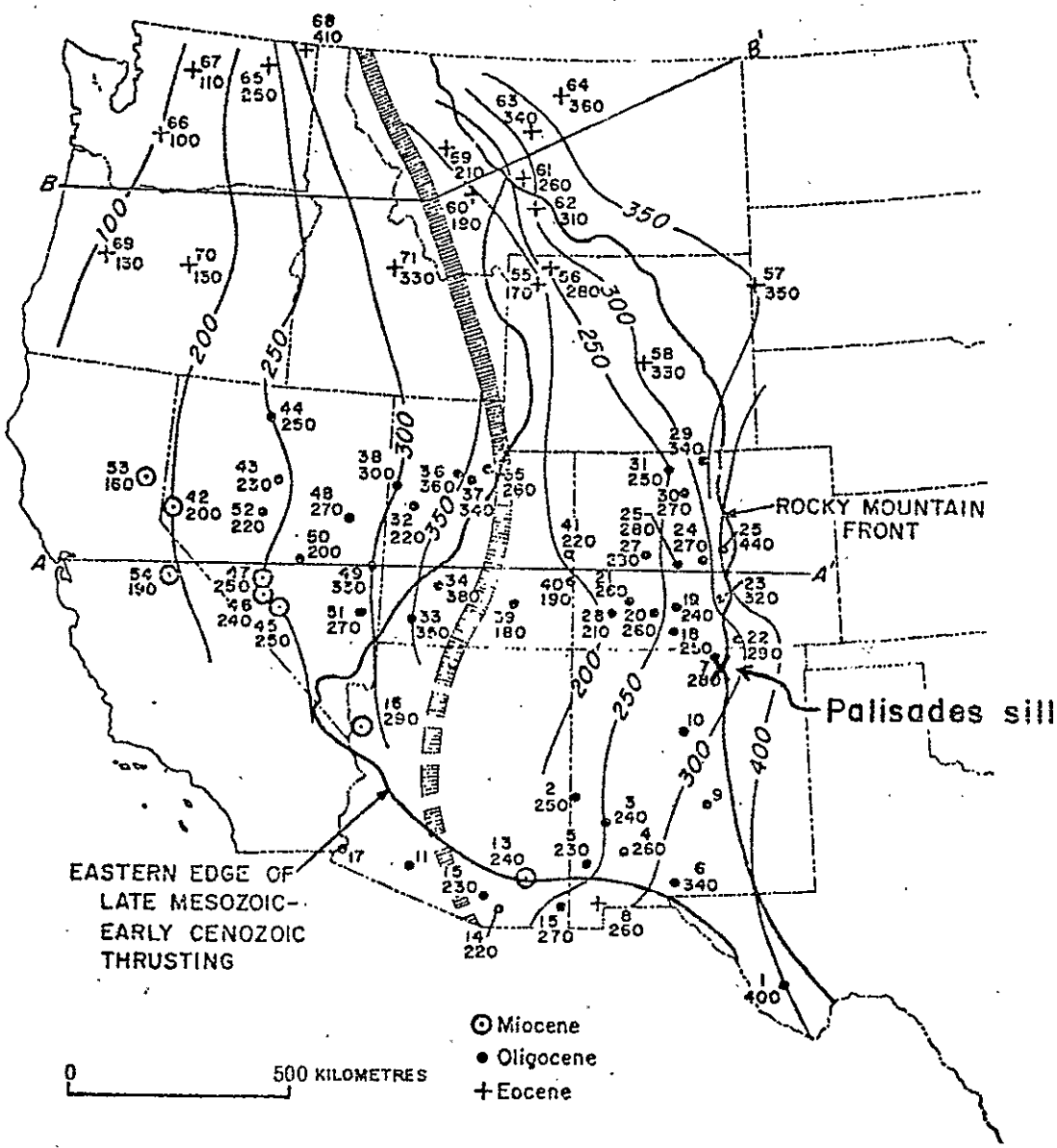

Figure 29. Spatial relationships of the Palisades sill to possible imbricate middle Cenozoic subduction zone (after Lipman and others, 1972, p. 235). Contoured depths (km) are to the subduction zone. Hachured line is a possible break between two subduction zones.

CONCLUSION

Figures 30 and 31 give a summary of mineralogic and chemical changes in the magma as a result of equilibrium crystallization and intrusion phenomenon of the Palisades sill. Assuming a model that primarily involves equilibrium crystallization, Figure 31 shows the variation in all chemical constituents in the magma with decreasing temperature. The sequence of events that occurred with decreasing temperature is as follows: 1) phenocryst crystallization (biotite, plagioclase, and quartz), 2) intrusion, 3) quartz resorption and groundmass crystallization, 4) quartz crystallization, and 5) partial dissolution (Fig. 30). As shown in Figure 31, there is considerable overlap of temperature range for these processes. Finally, Figure 31 shows the change in mineralogy of the sill with decreasing temperature.

Figure 30. Schematic diagram of phases and crystallization and alteration processes vs temperature of crystallization. Magnetite (less than 1 percent) is excluded. Temperature is very approximate - based on Figure 23 using data a 3 Kb assuming $P_{H_2O} = P_{total}$.

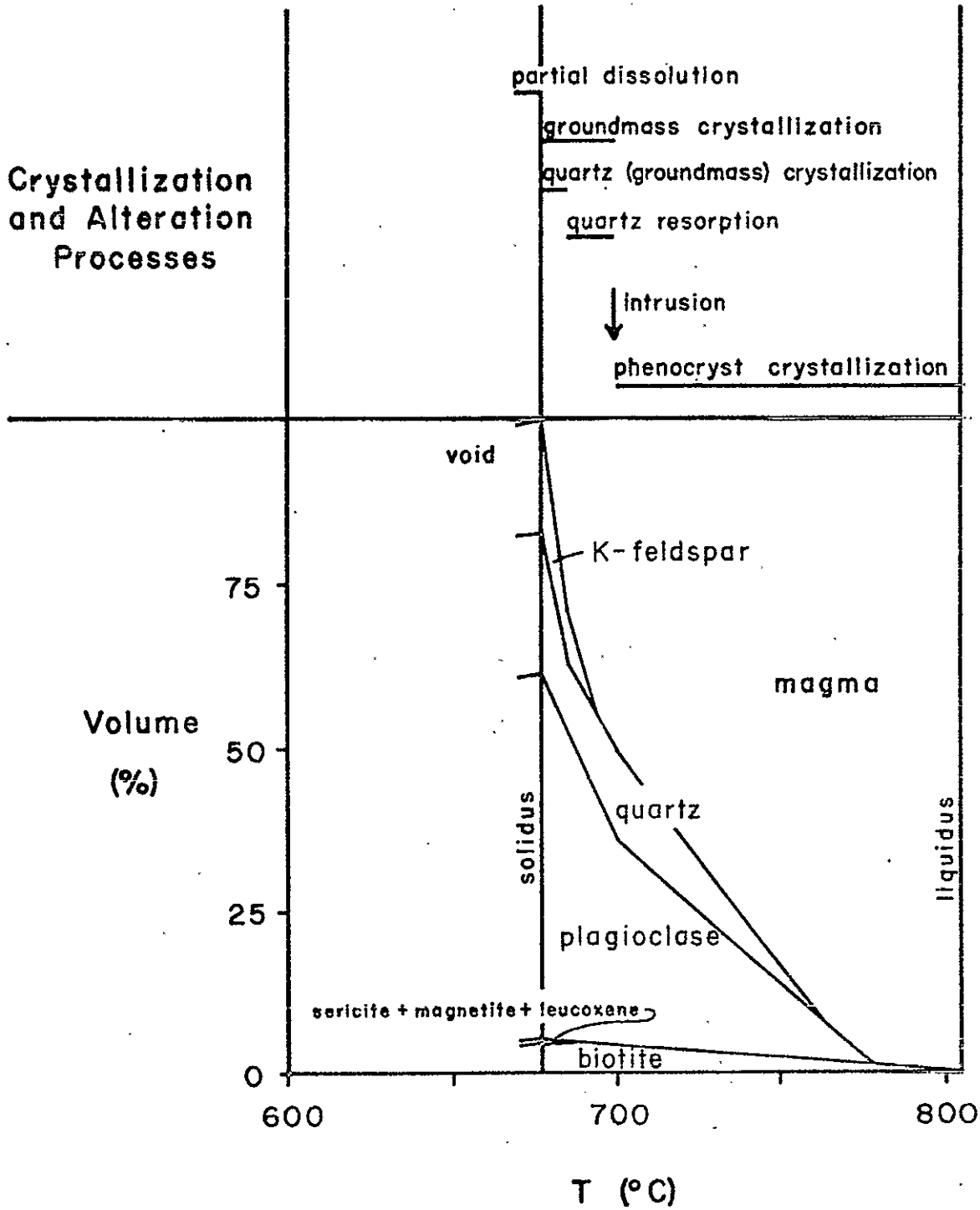
Crystallization and Alteration Processes
partial dissolution
groundmass crystallization
quartz (groundmass) crystallization
quartz resorption
intrusion
phenocryst crystallization
void
K-feldspar
magma
quartz
plagioclase
biotite
sericite + magnetite + leucoxene
solidus
liquidus
Volume (%)
75
50
25
0
600
700
800
T (°C)

Figure 31. Schematic diagram of oxide concentrations in the magma vs temperature of crystallization. TiO_2 is excluded. See Figure 30 for respective phases and crystallization and alteration processes.

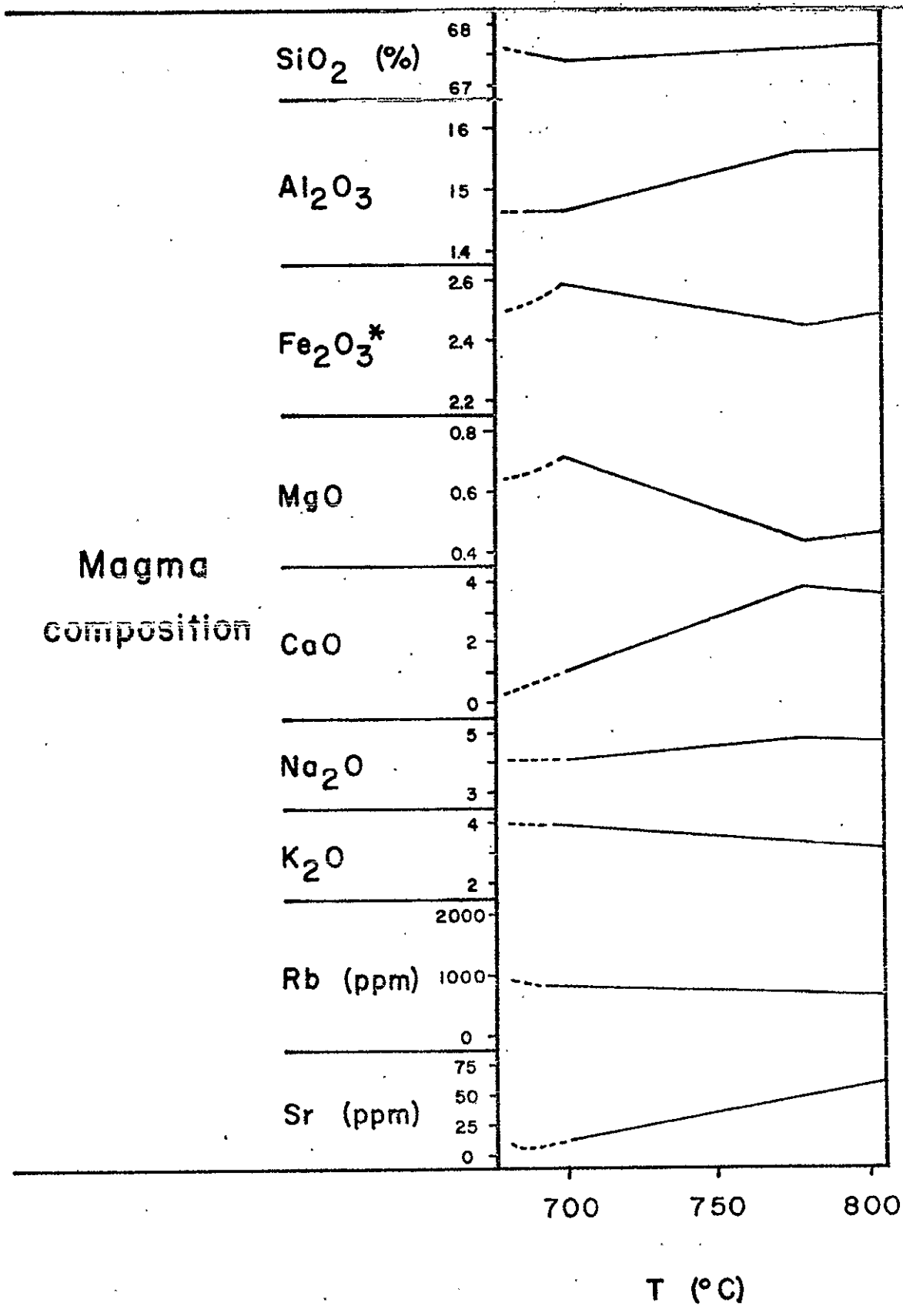
Magma composition
SiO2 (%)
68
67
Al2O3
16
15
14
Fe2O3*
2.6
2.4
2.2
MgO
0.8
0.6
0.4
CaO
4
2
0
Na2O
5
3
K2O
4
2
Rb (ppm)
2000
1000
0
Sr (ppm)
75
50
25
0
700
750
800
T (°C)

ACKNOWLEDGMENTS

The author wishes to express his appreciation to Dr. Paul C. Ragland for his assistance at all stages of this study, especially for his assistance in sample collection and his invaluable discussions after critically reading an early draft of this thesis.

Paul Drez of the University of North Carolina is thanked for his invaluable help concerning analytic procedures and for helpful discussions during the course of this study. Thanks are due to Steve Kish of the University of North Carolina for meaningful discussions. John Ragland, Caroline McLaughlin, and Susan Cannon are gratefully thanked for their assistance in sample collection. A special thanks goes to Susan Cannon for typing this thesis.

Harris, P. G., Kennedy, W. Q., and Carfe, C. M., 1970, Volcanism versus plutonism - the effect of chemical composition, in Newall, G., and Rast, N., eds., Mechanisms of Igneous Intrusions: Liverpool, Seel House Press, p. 187-200.

Hyndman, D. W., 1972, Petrology of igneous and metamorphic rocks: New York, McGraw-Hill Book Co., 533 p.

Lipman, P. W., Prostka, H. J., and Christiansen, R. L., 1972, Cenozoic volcanism and plate-tectonic evolution of the Western United States. Pt. I. Early and middle Cenozoic: Phil. Trans. R. Soc. Lond. A., v. 271, p. 217-248.

Nash, W. P., and Wilkinson, J. F. G., 1970, Shonkin Sag laccolith, Montana. Pt I. Mafic minerals and estimates of temperature, pressure, oxygen fugacity, and silica activity: Contr. Mineralogy and Petrology, v. 25, p. 241-269.

Northrop, S. A., and Read, C. B., 1966, Guidebook of Taos-Raton-Spanish Peaks country, New Mexico and Colorado: Socorro, New Mexico Geological Society, 128 p.

Piwinskii, A. J., 1968, Experimental studies of igneous rock series: Central Sierra Nevada Batholith, California: Jour. Geology, v. 76, p. 548-570.

_____, and Wyllie, P. J., 1968, Experimental studies of igneous rock series: a zoned pluton in the Wallowa Batholith, Oregon: Jour. Geology, v. 76, p. 205-234.

_____ 1970, Experimental studies of igneous rock series: felsic body suite from the Needle Point Pluton, Wallowa Batholith, Oregon, Jour. Geology, v. 78, p. 52-76.

Robinson, G. D., Wenek, A. A., Hays, W. H., and McCallum, M. C., 1964, Philmont country: U. S. Geol. Survey Prof. Paper 505, 152 p.

Salotti, C. A., and Matthews, V., 1969, Quartz-leached graphic-granite from Monticello, Georgia: Southeastern Geol., v. 10, p. 185-188.

Schwartz, G. M., 1958, Alteration of biotite under mesothermal conditions: Econ. Geology, v. 53, p. 164-177.

Shaw, H. R., 1965, Comments on viscosity, crystal settling, and convection in granitic magmas: Am. Jour. Sci., v. 263, p. 120-152.

Smith, J. F., and Ray, L. L., 1941, Geology of the Moreno Valley, New Mexico: Geol. Soc. America Bull., v. 52, p. 177-210.

REFERENCES CITED

Barker, D. S., and Burmester, R. F., 1970, Leaching of quartz from Precambrian hypabyssal rhyolite porphyry, Llano County, Texas: Contr. Mineralogy and Petrology, V. 28, p. 1-8.

Bartlett, R. W., 1969, Magma convection, temperature distribution, and differentiation: Am. Jour. Sci., v. 267, p. 1067-1082.

Bland, A. E., 1972, Geochemistry of the Meadow Flats complex, Orange County, North Carolina [M. S.] thesis: Chapel Hill, Univ. of North Carolina, 49 p.

Boyd, F. R., and England, J. L., 1960, The quartz-coesite transition: Jour. Geophys. Research, v. 65, no. 2, p. 749-756.

Brown, G. C., 1970, A comment on the role of water in the partial fusion of crustal rocks: Earth and Planetary Sci. Letters, v. 9, p. 355-358.

Burnham, C. W., and Jahns, R. H., 1962, A method for determining the solubility of water in silicate melts: Am. Jour. Sci., v. 260, p. 721-745.

Carmichael, I. S., Turner, F. J., and Verhoogen, J., 1974, Igneous Petrology: New York, McGraw-Hill Book Co., 739 p.

Eichelberger, J. C., 1975, Origin of andesite and dacite: evidence of mixing at Glass Mountain in California and at other circum-Pacific volcanoes: Geol. Soc. America Bull., v. 86, p. 1381-1391.

Eggler, D. H., 1974, Application of a portion of the system $CaAl_2Si_2O_8$-$NaAlSi_3O_8$-SiO_2-MgO-Fe-O_2-H_2O-CO_2 to genesis of the calc-alkaline suite: Am. Jour. Sci., v. 10, p. 297-315.

Flanagan, F. J., 1973, 1972 values for international geochemical samples: Geochim. et Cosmochim. Acta, v. 37, p. 1189-1200.

Fyfe, W. S., 1970, Some thoughts on granitic magmas, in Newall, G., and Rast, N., eds., Mechanisms of Igneous Intrusions: Liverpool, Seel House Press, p. 201-216.

Hall, A. L., 1932, The Bushveld igneous complex of the Central Transvaal: Geol. Surv. S. Africa Mem. 28.

_____ 1943, Geology of the Cimarron Range, New Mexico: Geol. Soc. America Bull., v. 54, p. 891-924.

Tauson, L. V., 1965, Factors in the distribution of the trace elements during the crystallization of magmas, in Ahrens, L. H., Press, F., Runcorn, S. K., and Urey, H. C., eds., Physics and chemistry of the earth, v. 6: Oxford, Pergamon Press, p. 215-259.

Taylor, S. R., 1965, The application of trace element data to problems in petrology, in Ahrens, L. H., Press, R., Runcorn, S. K., and Urey, H. C., eds., Physics and chemistry of the earth, v. 6: Oxford, Pergamon Press, p. 133-213.

Thornton, C. P., and Tuttle, O. F., 1960, Chemistry of igneous rocks. I. Differentiation index: Am. Jour. Sci., v. 258, p. 664-684.

Turekian, K. K., and Kulp, J. L., 1956, The geochemistry of strontium: Geochim. et Cosmochim. Acta, v. 10, p. 245-296.

Turner, F. J., 1968, Metamorphic Petrology: New York, McGraw-Hill Book Co., 403 p.

Tuttle, O. F., and Bowen, N. L., 1958, Origin of granite in the light of experimental studies in the system $NaAlSi_3O_8$-$KAlSi_3O_8$-SiO_2-H_2O: Geol. Soc. America Mem. 74, 153 p.

Van Der Plas, L., and Tobi, A. C., 1965, A chart for judging the reliability of point counting results: Am. Jour. Sci., v. 263, p. 87-90.

Wager, L. R., and Deer, W. A., 1939, Geological investigations in East Greenland. Pt. III. The petrology of the Skaergaard intrusion, Kangerdlugssuag, East Greenland: Medd. Greenland, v. 105, no. 4, p. 1-352.

Washington, H. S., 1917, Chemical analyses of igneous rocks published from 1884 to 1913: U. S. Geol. Survey Prof. Paper 99, 1201 p.

Winchell, A. N., and Winchell, H., Elements of Optical Mineralogy. Pt. II: New York, John Wiley & Sons, Inc., 551 p.

Winkler, H. G. F., 1974, Petrogenesis of metamorphic rocks: New York, Springer-Verlag, 320 p.

_____, Boese, M., and Marcopoulos, T., 1975, Low temperature granitic melts: N. Jb. Miner. Mh., p. 245-268.

Wooden, J. L., 1975, Geochemistry and Rb - Sr geochronology of Precambrian mafic dikes from the Beartooth, Ruby Range, and Tobacco Root Mountains, Montana [Ph.D.] dissert.: Chapel Hill, University of North Carolina, 194 p.

Wyllie, P. J., and Tuttle, O. F., 1961, Experimental investigation of silicate systems containing two volatile components. Pt. II. The effects of NH_3 and HF, in addition to H_2O on the melting temperatures of albite and granite: Am. Jour. Sci., v. 259, p. 128-143.

____ 1964, Experimental investigation of silicate systems containing two volatile components. Pt. III. The effects of SO_3, P_2O_5, HCl, and Li_2O, in addition to H_2O, on the melting temperatures of albite and granite: Am. Jour. Sci., v. 262, p. 930-939.

APPENDIX A: WHOLE ROCK CHEMICAL ANALYSIS

H-profile

sample number	SiO_2 (%)	Al_2O_3	Fe_2O_3	MgO	CaO	Na_2O	K_2O	TiO_2	total oxides	Rb (ppm)	Sr (ppm)
H1	67.93	16.14	2.88	0.75	1.72	5.50	2.96	0.30	98.18	693	46
H2	68.08	15.33	2.32	0.64	3.11	4.50	3.20	0.28	97.46	588	61
H3	67.28	16.64	2.10	0.64	2.90	4.38	3.44	0.28	97.66	467	64
H4	67.59	15.58	2.58	0.74	2.42	4.88	3.22	0.24	97.25	662	60
H5	66.81	15.93	2.54	0.86	2.66	4.40	3.52	0.28	97.00	434	61
H6	67.76	15.54	2.50	0.78	1.96	5.14	3.42	0.30	97.40	615	57
H7	68.10	15.71	2.47	0.63	2.24	5.38	3.18	0.27	97.98	983	52
H8	68.38	15.68	2.52	0.73	1.84	4.98	3.42	0.30	97.85	659	63
H9	68.28	15.77	2.48	0.76	2.18	5.14	3.32	0.28	98.21	767	54
H10	68.77	15.80	2.42	0.62	2.38	4.80	3.26	0.27	98.32	944	53
H11	67.14	15.65	2.57	0.96	3.05	4.62	3.40	0.26	97.55	776	57
H12	68.32	15.99	2.56	0.61	1.86	5.32	3.40	0.28	98.34	966	60
H13	68.84	16.05	2.55	0.54	1.63	5.38	3.40	0.28	98.67	985	57
H14	68.97	15.92	2.48	0.62	1.73	5.22	3.34	0.26	98.54	1076	59
H15	68.84	15.67	2.38	0.54	1.16	5.39	3.43	0.26	97.67	855	61
H16	68.74	15.65	2.60	0.66	1.52	5.43	3.38	0.30	98.28	1071	54
H17	69.00	15.75	2.50	0.70	1.33	5.29	3.40	0.30	98.27	697	60
H18	68.60	15.91	2.48	0.68	2.11	4.92	3.34	0.26	98.30	991	57
H19	66.90	15.67	2.46	0.72	2.42	4.83	3.40	0.27	96.67	468	56
H20	65.98	15.00	2.58	0.75	4.23	3.57	3.09	0.27	95.47	310	54
H21	67.66	15.61	2.48	0.68	1.73	5.48	3.27	0.28	97.19	684	58
H22	65.43	15.33	2.38	0.64	4.39	3.42	3.42	0.26	95.27	436	68
H23	68.22	15.63	2.35	0.66	3.06	4.36	3.35	0.26	97.89	690	62
H24	68.66	16.25	2.53	0.64	1.63	5.50	3.30	0.29	98.80	964	54
H25	67.74	15.67	2.48	0.53	3.57	4.43	3.16	0.27	97.85	640	60
H26	66.18	15.73	2.48	0.78	3.62	3.53	3.36	0.28	95.96	411	60
H27	68.16	16.33	2.62	0.64	2.45	4.92	3.34	0.30	98.75	831	64
H28	68.04	15.92	2.56	0.72	1.72	5.06	3.44	0.30	97.76	771	63
H29	68.52	15.75	2.45	0.64	2.98	4.54	3.18	0.24	98.30	884	58
H30	68.51	15.74	2.52	0.72	1.77	5.30	3.40	0.30	98.26	750	59
H31	69.10	15.84	2.58	0.71	2.07	5.01	3.18	0.27	98.75	904	56
H32	67.57	15.33	2.48	0.50	3.33	4.22	3.22	0.31	96.96	645	58
H33	66.68	15.40	2.48	0.24	3.43	3.88	3.54	0.27	95.92	508	71
H34	66.15	15.11	2.46	0.64	3.56	4.13	3.10	0.29	95.44	269	61
H35	66.14	15.43	2.42	0.59	3.40	4.23	3.12	0.28	95.61	251	54
H36	67.05	15.38	2.22	0.54	3.35	4.07	3.26	0.28	96.15	340	58
H37	66.48	15.89	2.42	0.68	3.11	4.54	3.24	0.29	96.65	507	61
H38	66.36	15.41	2.38	0.54	3.16	4.19	3.15	0.30	95.49	607	58
H39	67.04	15.49	2.36	0.56	3.46	3.91	3.34	0.31	96.47	523	63
H40	64.76	15.75	2.47	0.70	3.80	3.26	3.56	0.30	94.60	422	75

V-profile

sample number	SiO_2 (%)	Al_2O_3	Fe_2O_3	MgO	CaO	Na_2O	K_2O	TiO_2	total oxides	Rb (ppm)	Sr (ppm)
V1	66.33	15.41	2.38	0.68	3.52	3.95	3.28	0.27	95.81	562	62
V2	66.62	15.32	2.40	0.69	3.45	3.80	3.21	0.30	95.79	464	59
V3	68.43	15.56	2.46	0.74	3.01	4.51	3.36	0.27	98.34	912	55
V4	68.51	15.97	2.57	0.64	2.66	4.61	3.24	0.25	98.45	910	57
V5	68.91	15.58	2.49	0.68	2.66	4.43	3.28	0.27	98.30	893	61
V6	69.26	15.34	2.46	0.68	2.50	4.42	3.18	0.27	98.11	882	52
V7	68.24	15.81	2.44	0.55	2.63	4.64	3.20	0.26	97.77	940	56
V8	68.65	15.86	2.41	0.56	1.38	5.14	3.14	0.30	97.44	823	54
V9	68.36	15.58	2.48	0.72	2.78	4.48	3.30	0.28	97.98	780	59
V10	68.36	15.81	2.58	0.73	1.78	4.36	3.34	0.32	97.28	644	56
V11	68.22	15.98	2.46	0.70	2.76	4.54	3.24	0.28	98.18	909	57
V12	67.68	15.88	2.46	0.70	2.28	5.00	3.26	0.29	97.55	799	57
V13	68.68	15.77	2.48	0.60	1.73	5.36	3.32	0.27	98.21	922	60
V14	67.41	15.30	2.31	0.64	3.14	4.40	3.12	0.26	96.58	590	57
V15	66.08	15.61	2.44	0.78	3.37	4.44	3.18	0.30	96.20	617	59
V16	67.18	15.51	2.42	0.72	2.48	4.33	3.22	0.28	96.14	551	58
V17	66.40	15.73	2.46	0.66	3.17	4.50	3.30	0.28	96.50	606	59
V18	67.77	16.04	2.75	0.82	2.03	4.91	3.24	0.32	97.86	700	57
V19	68.04	16.17	3.02	0.86	3.00	4.79	3.06	0.32	99.26	909	58
V20	67.37	15.41	2.98	0.90	3.00	4.91	3.32	0.33	98.22	934	55
V21	67.53	16.49	2.81	0.76	1.00	5.46	3.35	0.34	97.74	655	56
V22	66.48	15.50	2.99	0.84	2.67	4.82	3.30	0.36	96.96	370	63
V23	71.96	14.33	1.02	0.16	1.64	4.18	3.98	0.07	97.34	486	122
V24	71.83	14.65	1.04	0.16	0.83	5.68	4.04	0.08	97.31	549	108
V25	69.27	15.31	1.50	0.24	1.83	4.44	3.20	0.29	96.08	677	57

APPENDIX B: "STRATIGRAPHIC" DISTANCE OF SAMPLES FROM LOWER CONTACT

H-profile

	actual distance		
H1	0.5		
H2	27.7		
H3	77.1		
H4	93.9		
H5	83.8		
H6	80.8	H26	271.9
H7	86.9	H27	277.4
H8	85.6	H28	282.5
H9	99.4	H29	289.0
H10	120.4	H30	303.0
H11	139.0	H31	311.8
H12	149.0	H32	324.3
H13	164.0	H33	332.5
H14	176.8	H34	346.3
H15	188.1	H35	353.0
H16	202.4	H36	357.2
H17	211.8	H37	366.7
H18	218.2	H38	378.9
H19	224.3	H39	381.9
H20	232.0	H40	382.8
H21	245.1		
H22	242.3		
H23	250.9		
H24	262.7		
H25	259.4		

V-profile

	actual distance	recalculated distance* (used in Thesis)
V1	0.3	0.3
V2	9.1	21.1
V3	18.3	20.4
V4	27.4	30.5
V5	42.9	47.9
V6	64.0	71.0
V7	75.0	83.5
V8	91.7	102.1
V9	106.3	118.3
V10	120.1	133.5
V11	134.7	149.7
V12	160.3	178.3
V13	174.9	194.5
V14	191.4	212.8
V15	206.0	228.9
V16	218.8	243.2
V17	231.6	257.6
V18	251.7	279.8
V19	262.4	291.7
V20	275.8	306.6
V21	292.6	325.2
V22	306.0	340.2
V23	319.7	355.4
V24	329.8	366.4
V25	343.5	381.6

APPENDIX C: ANALYTICAL PROCEDURES, PRECISION, AND ACCURACY

X-ray Fluorescence Analytical Information

Element	Tube	Crystal	Detector	Line	Comments
Si	Cr	PET	Flow proportional (gas)	$K_{\alpha 1,2}$	Fixed time count (10 sec.). Background not counted. Vacuum used.
Ca	Cr	PET	Flow proportional (gas)	$K_{\alpha 1,2}$	Fixed time count (10 sec.). Background not counted.
Ti	Cr	PET	Flow proportional (gas)	$K_{\alpha 1,2}$	Fixed time count (10 sec.). Background not counted. Vacuum used.
Sr	Mo	LiF (220)	Scintillation	$K_{\alpha 1,2}$	Fixed count of 10,000 and 40,000 on 3 backgrounds and 2 peaks, respectively.
Rb	Mo	LiF (220)	Scintillation	$K_{\alpha 1,2}$	Fixed count of 10,000 and 40,000 on 3 backgrounds and 2 peaks, respectively.

Atomic Absorption Analytical Information

Element	Line	Fuel / Oxident	Read Out
Na	Vis / 293.5	Acetelene / air	Null meter
K	Vis / 382.0	Acetelene / air	Null meter
Al	UV / 309.4	Acetelene / NO_2	Null meter
Mg	UV / 285.4	Acetelene / air	Null meter
Fe	UV / 249.3	Acetelene / air	Null meter

Accuracy

Major Element Results on Standards

		AGV	G1	W1	BCR
A*	SiO_2	59.00	69.19	52.64	54.48
B**		59.14	68.95	52.26	56.75
A	Al_2O_3	17.25	15.34	14.85	13.66
B		17.35	15.04	--	13.36
A	Fe_2O_3*	6.80	2.77	11.09	13.51
B		--	2.75	--	--
A	MgO	1.53	0.78	6.62	3.28
B		--	0.79	--	--
A	CaO	4.98	1.99	10.96	6.95
B		5.00	1.95	--	--
A	Na_2O	4.33	4.15	2.15	3.31
B		4.34	--	--	3.27
A	K_2O	2.90	4.51	0.64	1.68
B		2.96	4.51	0.61	--
A	TiO_2	1.08	0.53	1.07	2.23
B		--	0.52	--	--

* = Accepted value from Flanagan (1973).

** = This study.

Precision

	SiO_2	Al_2O_3	Fe_2O_3*	MgO	Na_2O	K_2O
Coefficient of Variation	0.32	0.90	0.90	1.33	0.61	0.67